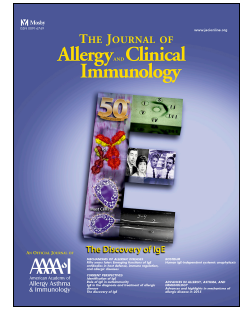


# Accepted Manuscript

Mechanisms of anaphylaxis in human low-affinity IgG receptor locus knock-in mice

Caitlin M. Gillis, B.Sci., Friederike Jönsson, PhD, David A. Mancardi, PhD, Naxin Tu, PhD, Héloïse Beutier, PharmD, Nico Van Rooijen, PhD, Lynn E. Macdonald, PhD, Andrew J. Murphy, PhD, Pierre Bruhns, PhD



PII: S0091-6749(16)30852-1

DOI: [10.1016/j.jaci.2016.06.058](https://doi.org/10.1016/j.jaci.2016.06.058)

Reference: YMAI 12301

To appear in: *Journal of Allergy and Clinical Immunology*

Received Date: 5 December 2015

Revised Date: 13 May 2016

Accepted Date: 13 June 2016

Please cite this article as: Gillis CM, Jönsson F, Mancardi DA, Tu N, Beutier H, Van Rooijen N, Macdonald LE, Murphy AJ, Bruhns P, Mechanisms of anaphylaxis in human low-affinity IgG receptor locus knock-in mice, *Journal of Allergy and Clinical Immunology* (2016), doi: 10.1016/j.jaci.2016.06.058.

This is a PDF file of an unedited manuscript that has been accepted for publication. As a service to our customers we are providing this early version of the manuscript. The manuscript will undergo copyediting, typesetting, and review of the resulting proof before it is published in its final form. Please note that during the production process errors may be discovered which could affect the content, and all legal disclaimers that apply to the journal pertain.

1 Mechanisms of anaphylaxis

2 **in human low-affinity IgG receptor locus knock-in mice**

3

4

5 Caitlin M. Gillis, B.Sci.<sup>1,2,3</sup>, Friederike Jönsson, PhD<sup>1,2</sup>, David A. Mancardi, PhD<sup>1,2</sup>,

6 Naxin Tu, PhD<sup>5</sup>, Héloïse Beutier, PharmD<sup>1,2,3</sup>, Nico Van Rooijen, PhD<sup>4</sup>, Lynn E.

7 Macdonald, PhD<sup>5</sup>, Andrew J. Murphy, PhD<sup>5</sup> and Pierre Bruhns, PhD<sup>1,2</sup>

8

9 **Authors' affiliations**

10 <sup>1</sup>Institut Pasteur, Department of Immunology, Unit of Antibodies in Therapy and

11 Pathology, Paris, France;

12 <sup>2</sup>INSERM, U1222, Paris, France;

13 <sup>3</sup>Université Pierre et Marie Curie, Paris, France;

14 <sup>4</sup>Department of Molecular Cell Biology, VU Medical Center, Amsterdam, The

15 Netherlands;

16 <sup>5</sup>Regeneron Pharmaceuticals, Inc., Tarrytown, NY, USA.

17

18 *Sources of funding: none of the sources of funding have an interest in the subject matter*

19 *or materials discussed in the submitted manuscript*

20

21 **Correspondence to:** Pierre Bruhns and Caitlin M. Gillis, Unit of Antibodies in Therapy

22 and Pathology, Department of Immunology, Institut Pasteur, 25 rue du Docteur Roux,

23 75015 Paris, France. Phone: +33144389146 or +33145688629. E-mail:

24 bruhs@pasteur.fr; caitlin.gillis@pasteur.fr

25

26

**ABSTRACT**

27 **Background:** Anaphylaxis can proceed through distinct IgE $\square$  or IgG $\square$  dependant  
28 pathways, which have been investigated in various mouse models. We developed a  
29 novel mouse strain in which the human low $\square$ affinity IgG receptor locus, comprising  
30 both activating (hFc $\gamma$ RIIA, hFc $\gamma$ RIIIA, hFc $\gamma$ RIIIB) and inhibitory (hFc $\gamma$ RIIB) hFc $\gamma$ R  
31 genes, has been inserted into the equivalent murine locus, corresponding to a locus  
32 'swap'.

33 **Objective:** We sought to determine the capabilities of hFc $\gamma$ Rs to induce systemic  
34 anaphylaxis, and identify the cell types and mediators involved.

35 **Methods:** hFc $\gamma$ R expression on mouse and human cells was compared to validate the  
36 model. Passive systemic anaphylaxis was induced by injection of heat $\square$ aggregated  
37 human IVIG, and active systemic anaphylaxis following immunisation and challenge.  
38 Anaphylaxis severity was evaluated by hypothermia and mortality. The contribution of  
39 receptors, mediators or cell types was assessed by receptor blockade or depletion.

40 **Results:** The human to mouse low $\square$ affinity Fc $\gamma$ R locus swap engendered  
41 hFc $\gamma$ RIIA/IIB/IIIA/IIIB expression in mice comparable to that in humans. Knock $\square$ in  
42 mice were susceptible to passive and active anaphylaxis, accompanied by  
43 downregulation of both activating and inhibitory hFc $\gamma$ R expression on specific myeloid  
44 cells. The contribution of hFc $\gamma$ RIIA was predominant. Depletion of neutrophils  
45 protected against hypothermia and mortality. Basophils contributed to a lesser extent.  
46 Anaphylaxis was inhibited by Platelet-Activating Factor receptor or Histamine receptor-  
47 1 blockade.

48 **Conclusion** : Low affinity FcγR locus-switched mice represent an unprecedented  
49 model of cognate hFcγR expression. Importantly, IgG anaphylaxis proceeds within a  
50 native context of activating and inhibitory hFcγRs; indicating that, despite robust  
51 hFcγRIIB expression, activating signals can dominate to initiate a severe anaphylactic  
52 reaction.

53

54

55

56

**CLINICAL IMPLICATIONS**

57 In a mouse model of cognate human IgG receptors expression, hFcγR engagement with  
58 IgG immune complexes induced severe anaphylaxis. These findings benefit the  
59 understanding of human IgG-dependent anaphylaxis, whether non-classical (IgE-  
60 independent) or following IgG-based therapies.

61

62

63

**CAPSULE SUMMARY**

64

65 Antibodies of the IgG class can contribute to anaphylaxis. This report reveals that  
66 human IgG receptor knock-in mice are susceptible to systemic anaphylaxis,  
67 demonstrating the predominance of activating over inhibitory IgG receptors and the  
68 major contribution of human FcγRIIA, neutrophils and platelet-activating factor.

69

70

**KEY WORDS**

71

72 Anaphylaxis; IgG; knock-in mouse model; basophil; neutrophil; monocyte;  
73 macrophage; human FcγR; Platelet-activating Factor; Histamine.

74

75

76 **ABBREVIATIONS USED**

77

78 Fc $\gamma$ R: IgG Fc receptor

79 PAF: Platelet-Activating Factor

80 WT: Wild-Type

81 PSA: Passive Systemic Anaphylaxis

82 ASA: Active Systemic Anaphylaxis

83 BSA: Bovine Serum Albumin

84 HA: heat-aggregated

85 mAb: monoclonal Antibody

86 PBS: Phosphate Buffered Saline

87 BBS: Borate Buffered Saline

88 GeoMean: Geometric Mean

89 SEM: Standard Error of the Mean

90

91

**INTRODUCTION**

92

93

Anaphylaxis is a severe, systemic allergic reaction, the reported incidence of which is increasing worldwide<sup>1-3</sup>. Reactions are clinically heterogeneous, yet characterised by rapid symptom progression and risk of death: intense vasodilation and bronchoconstriction can lead to hypotension, hypothermia, tachycardia, and respiratory distress, which may result in heart and lung failure. In children the most common causative agent is food, whereas in adults drug-induced anaphylaxis accounts for the majority of cases, and indeed the majority of fatal reactions. Anaphylaxis is classically attributed to an IgE-mediated reaction driven by mast cell activation and release of histamine and tryptase<sup>4</sup>.

100

101

102

103

104

105

106

107

108

109

110

111

112

113

114

Many cases of human anaphylaxis, in particular to drugs, are not accompanied by elevated serum tryptase or detectable antigen-specific IgE<sup>5-8</sup>. Alternative, IgE-independent pathways may actually underlie a significant fraction of these anaphylactic events: indeed, non-IgE reactions have been reported to account for up to 30% of cases of drug-induced anaphylaxis<sup>9</sup>. Furthermore, measures of histamine and mast cell tryptase in patients' sera do not reflect the severity of reactions<sup>7, 10</sup>, whereas serum platelet-activating factor (PAF) levels were found to directly correlate with anaphylaxis severity<sup>11, 12</sup>. Supporting these notions, experimental animal models have demonstrated that fatal systemic anaphylaxis following intravenous challenge proceeds via PAF release triggered by non-IgE-dependant pathways, and in particular by IgG-dependant pathways (reviewed in <sup>13, 14</sup>). The respective contribution of IgE- and IgG-mediated pathways in human anaphylaxis remains however to be determined.

115           Passive systemic anaphylaxis (PSA) may be induced in mice by the transfer of  
116 specific IgE or IgG antibodies prior to a challenge with a specific antigen, or by the  
117 transfer of pre-formed IgG immune complexes. Active systemic anaphylaxis (ASA) is  
118 elicited by immunisation with an antigen prior to challenge with the same antigen; a  
119 polyclonal IgE and IgG antibody response is generated, and death can result from  
120 antigen challenge. In both models, use of the intravenous route for allergen challenge  
121 mimics drug-induced anaphylaxis in patients. ASA does not depend on IgE antibodies,  
122 activating IgE receptors, or mast cells<sup>15, 16</sup>, but rather requires activating IgG receptors  
123 (Fc $\gamma$ R), and the contribution of other myeloid cells: neutrophils, basophils or  
124 monocyte/macrophages<sup>17-19</sup>. Platelet-activating factor (PAF) was identified as the  
125 dominant downstream mediator of IgG-induced anaphylaxis, and PAF alone, like  
126 histamine, can reproduce the signs and symptoms of anaphylaxis<sup>20, 21</sup>. Thus mouse  
127 models suggest a pathway of anaphylaxis driven by IgG-mediated activation of myeloid  
128 cells and relying on PAF release.

129

130           Allergic patients that possess detectable allergen-specific IgE also possess  
131 detectable allergen-specific IgG. These anti-allergen IgG antibodies are mainly of the  
132 IgG1 isotype, whereas anti-allergen IgG4 antibodies increase following allergen  
133 immunotherapy<sup>22-25</sup>. Allergen-specific IgG4 levels are considered a good correlate to  
134 successful allergen immunotherapy, however it remains unknown if allergen-specific  
135 IgG1 participate in, or are even responsible for, non-IgE mediated human anaphylaxis.  
136 Humans express a family of IgG receptors (Fc $\gamma$ R), comprised of activating IgG  
137 receptors (hFc $\gamma$ RI/CD64, hFc $\gamma$ RIIA/CD32A, hFc $\gamma$ RIIC/CD32C, hFc $\gamma$ RIIIA/CD16A,  
138 hFc $\gamma$ RIIIB/CD16B) and a single inhibitory receptor (hFc $\gamma$ RIIB/CD32B), that all bind  
139 human IgG1 and that mediate most of the biological functions of IgG<sup>26</sup>. Although mice



140 also express both activating and inhibitory Fc $\gamma$ Rs, murine Fc $\gamma$ Rs do not structurally or  
141 functionally mirror those of humans: differential antibody binding affinities and  
142 variable expression on immune cell subsets prevent extrapolation from one species to  
143 another<sup>26</sup>. We reported previously the induction of anaphylaxis (PSA and fatal ASA) in  
144 mice transgenic either for hFc $\gamma$ RI/CD64 or hFc $\gamma$ RIIA/CD32A on a background  
145 deficient in endogenous mFc $\gamma$ R<sup>19, 27</sup>. PSA mediated by hFc $\gamma$ RIIA was independent of  
146 mast cells and basophils, and relied on neutrophils and monocytes/ macrophages<sup>28</sup>, and  
147 hFc $\gamma$ RI-dependent ASA required neutrophils and PAF release<sup>27</sup>. An important caveat of  
148 these results is that they were obtained in mice expressing only one hFc $\gamma$ R, in the  
149 absence of potential regulatory or cooperative effects of other hFc $\gamma$ Rs. In a model  
150 generated by intercrossing of five different hFc $\gamma$ R-transgenic mice, incorporating  
151 activating and inhibitory hFc $\gamma$ Rs, administration of aggregated human IgG to [hFc $\gamma$ RI<sup>tg</sup>  
152 hFc $\gamma$ RIIA<sup>tg</sup> hFc $\gamma$ RIIB<sup>tg</sup> hFc $\gamma$ RIIIA<sup>tg</sup> hFc $\gamma$ RIIIB<sup>tg</sup>] mice on a mFc $\gamma$ R<sup>null</sup> background was  
153 sufficient to trigger anaphylaxis, although the mechanisms were not addressed<sup>29</sup>. This  
154 model reproduces, however, aberrant expressions seen in mice carrying the individual  
155 transgenes, including extremely high expression of hFc $\gamma$ RIIB on mouse monocytes and  
156 granulocytes<sup>26</sup>.

157

158 Here, we present a novel mouse model in which we have employed highly  
159 efficient knock-in technology to insert the entire low-affinity hFc $\gamma$ R locus into the  
160 corresponding mouse locus on chromosome 1. This approach engendered expression of  
161 activating hFc $\gamma$ RIIA/CD32A, hFc $\gamma$ RIIIA/CD16A and hFc $\gamma$ RIIIB/CD16B, and of  
162 inhibitory hFc $\gamma$ RIIB/CD32B in mice, in a manner resembling expression patterns seen  
163 in humans. This unprecedented model permits analyses of the role of hFc $\gamma$ Rs and the

164 cell types that express them in IgG-mediated anaphylaxis, within a cognate context of  
165 activating and inhibitory hFcγRs.

166

ACCEPTED MANUSCRIPT

167

**METHODS**

168

**Mice**

169 VG1505 and VG1543 mice were designed and generated by Regeneron  
170 Pharmaceuticals, Inc. on a mixed 62.5% C57BL/6N, 37.5% 129S6/SvEv genetic  
171 background (refer to Supplemental Methods), and backcrossed one generation to  
172 C57BL/6N. Mice were bred at Institut Pasteur and used for experiments at 7-11 weeks  
173 of age. VG1505 and VG1543 mice demonstrate normal development and breeding  
174 patterns. All mouse protocols were approved by the Animal Ethics committee CETEA  
175 (Institut Pasteur, Paris, France) registered under #C2EA-89.

177

**Active Systemic Anaphylaxis**

178 Mice were injected intraperitoneally on day 0 with 200µg BSA in CFA, and boosted  
179 intraperitoneally on day 14 with 200µg BSA in IFA. BSA-specific IgG1, IgG2a/b/c and  
180 IgE antibodies in serum were titered by ELISA on day 21 as described<sup>19</sup>. Mice with  
181 comparable antibody titers were challenged intravenously with 500µg BSA 10-14 days  
182 after the last immunisation. Central temperature was monitored using a digital  
183 thermometer (YSI) with rectal probe.

185

**Passive Systemic Anaphylaxis**

186 Human Intravenous Immunoglobulin (IVIG; Gamunex®, Grifols) was heat-aggregated  
187 by incubation at 25mg/mL in BBS (0.17M H<sub>3</sub>BO<sub>3</sub>, 0.12M NaCl, pH8) for 1 hour at  
188 63°C, then diluted in 0.9% NaCl for iv injection at 100µL per mouse. Central  
189 temperature was monitored using a digital thermometer with rectal probe. Control non-  
190 aggregated IVIG was similarly diluted without heating. For hFcγR expression analysis  
191

192 following IVIG-PSA, heparinised blood was sampled 1hour after IVIG injection. IgE-  
193 dependant PSA was induced by challenge with 500µg TNP-BSA 16 hours after passive  
194 transfer of IgE anti-TNP (50µg clone C48.2). PSA was induced also by PAF injection at  
195 0.3µg per mouse i.v., and hypothermia monitored immediately afterwards.

196

### 197 **In vivo blocking and depletion**

198 Anti-FcγRIIA mAbs (Clone IV.3, 60µg /mouse) were injected twice intravenously (24  
199 hours and 4 hours) before challenge. Note that, unlike in FcγRIIA<sup>tg</sup> mice<sup>30</sup>, IV.3  
200 administration did not induce hypothermia or symptoms of anaphylaxis, nor platelet  
201 depletion. 300µg /mouse anti-Gr-1 (RB6-8C5), 300µg /mouse anti-Ly-6G (NIMP-R14),  
202 30µg/mouse (Supplementary Figure 5A&D, Supplementary Figure 6B) or 60µg/mouse  
203 anti-CD200R3 (Ba103) (Figure 4E), 300µg /mouse anti-Ly-6C (Monts 1, rat IgG2a)  
204 mAbs, or corresponding rat IgG2b or IgG2a isotype control mAbs were injected  
205 intravenously 24 hours before challenge. Note that the NIMP-R14 antibody clone is  
206 specific to the Ly-6G antigen (Supplementary Figure 4A-C). 300µL /mouse PBS- or  
207 clodronate-liposomes were injected intravenously either 24 hours before challenge, or  
208 both 24 and 48 hours before challenge. Specificity of cell depletion was evaluated in the  
209 blood, spleen and peritoneal lavage of naive 1543 mice 24 hours after NIMP-R14  
210 (Supplementary Figure 4C-E) or Ba103 (Supplementary Figure 5). Please refer to  
211 *“Specificity and efficiency of cell depletion strategies” in the Supplemental Methods for*  
212 *more information.*

213 PAF-R antagonists ABT-491 (25µg/mouse) or CV-6209 (66µg/mouse) in 0.9% NaCl  
214 were injected intravenously 15min or 10min prior to challenge, respectively. H1-  
215 receptor antagonists cetirizine DiHCl, pyrilamine maleate , or triprolidine HCl at  
216 300µg/mouse in 0.9% NaCl were injected intraperitoneally 30 minutes before challenge.

217

218 *Please refer to Supplemental Methods for details on: Generation of knock-in mice,*

219 *Antibodies and reagents, Flow cytometry, Specificity and efficiency of cell depletion*

220 *strategies, Statistics.*

221

ACCEPTED MANUSCRIPT

222

**RESULTS**

223

224 **Creation of VG1505 (mFcγRIIB<sup>-/-</sup> mFcγRIII<sup>-/-</sup> mFcγRIV<sup>-/-</sup>) and VG1543**  
225 **(mFcγRIIB<sup>-/-</sup> mFcγRIII<sup>-/-</sup> mFcγRIV<sup>-/-</sup> hFcγRIIA<sup>KI</sup> hFcγRIIB<sup>KI</sup> hFcγRIIIA<sup>KI</sup>**  
226 **hFcγRIIIB<sup>KI</sup>) mice**

227 To delete the mouse low-affinity Fc receptors, a large targeting vector  
228 (BACvec)<sup>31, 32</sup> was constructed (as described in supplemental methods) to delete 106 kb  
229 of mouse genomic sequence encompassing the mouse Fcgr2b, Fcgr3, and Fcgr4 genes,  
230 and used to target VGF1 ES cells<sup>33</sup>. The low-affinity FcγR deleted allele (deletion of  
231 1:170,956,770-171,063,353 from Chr1\_H3 based on the mouse GRCh38 assembly) was  
232 given the designation VG1505 (Figure 1A).

233 To insert human FCGR3A and FCGR2A genes, a BACvec containing 69 kb of  
234 the corresponding human sequence flanked by long mouse homology arms was  
235 generated (refer to Supplemental Methods) and used to retarget VG1505 ES cells<sup>31</sup>. The  
236 subsequent allele in which the three mouse low affinity Fc receptors were replaced with  
237 hFCGR3A and hFCGR2A was given the designation VG1528 (Figure 1B). To insert  
238 human FCGR2B, FCGR2C and FCGR3B genes next to the human FCGR3A and  
239 FCGR2A genes, a BACvec was constructed containing an additional 142 kb of human  
240 sequence between a human homology arm, homologous to the end of the human insert  
241 in VG1528, and a mouse homology arm. This BACvec was used to retarget VG1528 ES  
242 cells, and resulted in an allele designated VG1543<sup>31, 32</sup> (insertion of human sequence  
243 from 1:161,500,441-161,679,348 on Chr1\_q23.3 based on the human GRCh38  
244 assembly) in which all five human low-affinity FcγR receptor genes replace the three  
245 mouse low-affinity FcγR genes (Figure 1C). The inserted human low-affinity FcγRs are  
246 in the same order as in the human genome and the human intergenic sequences are

247 retained intact. The human BAC sequences used encode for the polymorphic variants  
248 hFcγRIIA(H<sub>131</sub>), hFcγRIIB(I<sub>232</sub>), hFcγRIIC(Stop<sub>13</sub>), hFcγRIIIA(V<sub>158</sub>) and  
249 hFcγRIIIB(NA2); therefore no expression of hFcγRIIC is expected in VG1543 mice.

250

251 **VG1543 mice exhibit hFcγR expression patterns on immune cells comparable to**  
252 **that of humans**

253 First, we determined that VG1505 and VG1543 mice exhibit normal immune  
254 cell composition (Supplementary Table 4). VG1505 mice demonstrate slightly elevated  
255 frequencies of granulocytes and monocytes in the blood and spleen, and macrophages in  
256 the peritoneum compared to VG1543 (Supplementary Figure 1A-C). Furthermore,  
257 VG1505 and VG1543 mice exhibit comparable mFcεRI and mFcγRI expression  
258 (Supplementary Figure 1D-F).

259 To compare the expression pattern of hFcγRs in VG1543 mice to that of humans,  
260 specific antibody staining and flow cytometry analysis was performed on cells isolated  
261 either from the blood of healthy human donors, or from the blood, spleen, lymph nodes,  
262 bone marrow, peritoneum and broncho-alveolar lavage (BAL) of VG1543 mice. All  
263 myeloid cells examined, including monocytes, macrophages, eosinophils, basophils and  
264 mast cells, and among lymphocytes B and NK cells, but not T cells, expressed at least  
265 one hFcγR (Figure 2A-B).

266 We detected hFcγRIIA (CD32A) staining on neutrophils, monocytes,  
267 eosinophils and platelets from the blood of healthy human donors (Figure 2A) as  
268 expected<sup>26</sup>, and from the blood, spleen, lymph nodes, bone marrow, peritoneum and  
269 broncho-alveolar lavage of VG1543 mice (Figure 2B). VG1543 peritoneal mast cells  
270 also expressed hFcγRIIA. Like human blood basophils, VG1543 blood basophils  
271 expressed variably hFcγRIIA (Figure 2A-B), but not basophils from the spleen or bone

272 marrow; the low level of expression of hFcγRIIA on VG1543 blood basophils is in the  
273 range of expression found on basophils from human donors (Figure 2C). As expected,  
274 lymphocytes, including B, T and NK cells, did not express hFcγRIIA in humans and  
275 VG1543 mice (Figure 2A-B); notably we observed some background staining for  
276 hFcγRIIA on human B cells, as published previously<sup>28</sup>. Thus the hFcγRIIA expression  
277 pattern and level is comparable between VG1543 mice and blood from normal human  
278 donors.

279 In human blood hFcγRIIB was detected at high levels on all B cells and basophils,  
280 at lower levels variably on a proportion of monocytes (2-38% positive; n=4 donors),  
281 whereas other cells were mostly negative, *i.e.* neutrophils, eosinophils, NK cells, T cells,  
282 platelets (Figure 2A and Supplemental Figure 1A), as expected<sup>34, 35</sup>. Similarly, VG1543  
283 mice expressed high levels of hFcγRIIB on B cells from blood, spleen, lymph node and  
284 peritoneum (Figure 2B). Furthermore, we observed variation in hFcγRIIB staining  
285 among B cell subpopulations isolated from the bone marrow and the peritoneum of  
286 VG1543 mice (Supplementary Figure 1B-C). VG1543 mice demonstrated robust  
287 hFcγRIIB expression on monocyte populations in the blood and lymphoid organs, yet  
288 no staining was observed on Ly6C<sup>hi</sup> monocytes from the bone marrow. Only a fraction  
289 of donors we analysed demonstrated hFcγRIIB expression on blood monocytes  
290 (Supplemental Figure 2A), consistent with its previously reported variable expression  
291 on CD14<sup>lo</sup> monocytes and absence of expression on CD14<sup>hi</sup> monocytes<sup>36</sup>. Thus VG1543  
292 exhibit over-expression of hFcγRIIB on blood monocytes compared to human blood  
293 monocytes. Interestingly, hFcγRIIB staining was higher on Ly6C<sup>low</sup> “patrolling”  
294 monocytes than on Ly6C<sup>hi</sup> “classical” monocytes from VG1543 mice (Supplemental  
295 Figure 2D), as it is on the analogous populations in human blood, CD14<sup>low</sup>CD16<sup>hi</sup>  
296 “patrolling” monocytes and CD14<sup>hi</sup> “classical” monocytes (Supplemental Figure 2E).



297 Furthermore, spleen monocytes in human<sup>36</sup> and VG1543 mice express significant levels  
298 of hFcγRIIB, reconciling hFcγRIIB expression on monocytes in this compartment  
299 between human donors and VG1543 mice. Macrophages from the peritoneum, but not  
300 from BAL, of VG1543 mice were found positive for hFcγRIIB (Figure 2B). Although  
301 human basophils express high levels of hFcγRIIB<sup>37</sup>, basophils from VG1543 mice were  
302 negative (Figure 2A-B). Overall, VG1543 mice appear to express hFcγRIIB at similar  
303 levels on B cells, at the high end of the range on monocytes, but not on basophils,  
304 compared to humans.

305 Human neutrophils, monocytes, eosinophils, NK cells and a small proportion of  
306 basophils were labelled positive with an anti-CD16 antibody recognizing both  
307 hFcγRIIIA and hFcγRIIIB (Figure 2A), in accordance with known hFcγRIIIA (NK cells,  
308 monocytes/macrophages and eosinophils) and hFcγRIIIB expression (neutrophils and  
309 some basophils)<sup>35</sup>. Similarly, in the blood and organs from VG1543 mice, neutrophils  
310 stained at high levels, and monocyte/macrophages, NK cells and basophils at variable  
311 levels with anti-CD16 (Figure 2B and Supplemental Figure 1). Eosinophils from  
312 VG1543 mice did not show detectable CD16 labelling, in accordance with 25% of  
313 human donors (Supplemental Figure 1F). Interestingly, CD16 was apparent on only 30-  
314 45% of NKp46<sup>+</sup> NK cells from the spleen of VG1543 mice, compared to 85-98% of  
315 CD56<sup>+</sup> NK cells from human blood. Overall, VG1543 mice appear to express  
316 hFcγRIIIA and hFcγRIIIB at similar levels on neutrophils and NK cells, at higher levels  
317 on blood monocytes, but not on eosinophils nor on blood basophils, respectively,  
318 compared to humans.

319

320 **Induction and mechanism of active systemic anaphylaxis in VG1543 mice**

321 Among human low-affinity hFcγRs, the activating IgG receptors hFcγRIIA and  
322 hFcγRIIIA, and the inhibitory IgG receptor hFcγRIIB, can bind mouse IgG isotypes<sup>26, 28,</sup>  
323 <sup>35</sup> (Table 1): we therefore explored the capacity of these receptors to mediate active  
324 systemic anaphylaxis (ASA) triggered by i.v. BSA challenge in VG1505 and VG1543  
325 mice immunised with BSA (Supplemental Figure 3). Following challenge, VG1543  
326 mice, but not in VG1505 mice, suffered from a severe drop in body temperature and 50-  
327 100% mortality within 30 minutes (Figure 3A). Pre-treatment of VG1543 mice with  
328 blocking antibodies against activating hFcγRIIA (mAb IV.3)<sup>28</sup> abolished hypothermia  
329 and mortality (Figure 3B). hFcγRIIA is expressed by neutrophils,  
330 monocyte/macrophages, eosinophils, basophils and mast cells in VG1543 mice. Of  
331 these, neutrophils, monocyte/macrophages and basophils have been reported to  
332 contribute to IgG-PSA in mice<sup>17-19</sup>. Neutrophil depletion using either anti-Ly6G or anti-  
333 Gr1 mAbs protected VG1543 mice from ASA, but neither monocyte/macrophage nor  
334 basophil depletion (Figure 3C; Supplemental Figure 5B-E). Finally, PAF-receptor  
335 blockade protected from ASA-associated death and hypothermia, while H1-receptor  
336 antagonist cetirizine had no effect (Figure 3D, Supplemental Figure 5F-G). Altogether  
337 these data, obtained in this model of ASA contingent on hFcγR binding of mouse IgGs,  
338 demonstrate that VG1543 mice present with anaphylactic symptoms and a fatal reaction  
339 dependent on hFcγRIIA, neutrophils and PAF. They also demonstrate that mouse FcγRI,  
340 which is still expressed in both VG1505 mice and VG1543 mice, cannot induce  
341 anaphylaxis.

342

### 343 **Aggregated human IVIG triggers passive systemic anaphylaxis in VG1543 mice**

344 Although interactions between mouse IgG isotypes and some human FcγRs can  
345 result in the induction of anaphylactic reactions (Figure 3, Table 1 and <sup>19, 27, 28</sup>), such

346 models are far from recapitulating the variety of human IgG interactions with both  
347 activating and inhibitory hFcγRs<sup>38</sup>. We therefore investigated whether anaphylaxis  
348 could be initiated by triggering human FcγRs in VG1543 mice using aggregated human  
349 intravenous immunoglobulin (IVIG) as a surrogate for human IgG-immune complexes.  
350 Intravenous injection of 1mg heat-aggregated IVIG induced passive systemic  
351 anaphylaxis (IVIG-PSA) in VG1543 mice, manifested by visual signs and severe  
352 hypothermia, with a maximum temperature loss of 6-8°C 30-40 min after injection. This  
353 reaction was dependant on the expression of hFcγR, since VG1505 mice were resistant  
354 (Figure 4A). A dose response of heat-aggregated IVIG demonstrated that hypothermia  
355 reaches a maximum at 1 mg, was lower at 500 or 300 µg, and was not observed at 30 µg  
356 (Figure 4B & Supplemental Figure 4). A dose of 1mg was therefore chosen for all  
357 subsequent IVIG-PSA, as it consistently induced in VG1543 mice a shock at sufficient  
358 magnitude to assess the effect of receptor, cell and mediator blockade.

359

### 360 **hFcγRIIA and neutrophils contribute to IVIG-PSA in VG1543 mice**

361 hFcγRIIA blockade protected against both anaphylactic symptoms and  
362 hypothermia during IVIG-PSA in VG1543 mice, (Figure 4C), even though VG1543  
363 mice express also hFcγRIIA and hFcγRIIB that may induce cell activation<sup>26, 35, 39</sup>.  
364 Monocyte/macrophage depletion by toxic liposome administration had no effect (Figure  
365 4D), whereas basophil depletion modestly reduced IVIG-PSA in VG1543 mice (Figure  
366 4E). Neutrophil depletion, however, was protective (Figure 4F). Appropriate antibody-  
367 mediated cell depletion was confirmed by flow cytometry analysis (Supplemental  
368 Figure 4 and 5A), and we have previously demonstrated efficient monocyte/macrophage  
369 depletion in the blood and spleen following liposome injection (Beutier et al 2016).  
370 hFcγRIIB blockade, even using high doses of blocking mAb, did not modulate

371 anaphylactic symptoms in VG1543 mice induced by optimal (1mg; not shown) or  
372 suboptimal (250 $\mu$ g; Figure 4G) doses of heat-aggregated IVIG. Thus VG1543 mice are  
373 susceptible to PSA induced by human IgG, and the reaction proceeds primarily through  
374 neutrophils and the activating receptor hFc $\gamma$ RIIA, with a minor contribution of  
375 basophils, but does not require monocyte/macrophages, and is not negatively regulated  
376 by inhibitory hFc $\gamma$ RIIB.

377

### 378 **Changes in hFc $\gamma$ R expression on myeloid cells following anaphylaxis**

379 It has been proposed that changes in Fc receptor expression may be used as a  
380 biological marker for anaphylaxis, or an indicator of different pathways of activation<sup>40</sup>.  
381 We therefore investigated changes in hFc $\gamma$ R expression on circulating myeloid cell  
382 populations following IVIG-PSA in VG1543 mice. One hour after anaphylaxis  
383 induction, staining for activating hFc $\gamma$ R receptors was substantially reduced on  
384 neutrophils (Figure 5A), Ly6C<sup>hi</sup> (Figure 5B) and Ly6C<sup>low</sup> monocytes (Figure 5C) in the  
385 blood of VG1543 mice; entailing almost complete loss of hFc $\gamma$ RIIA on neutrophils and  
386 monocytes, and significant downregulation of hFc $\gamma$ RIII on neutrophils and Ly6C<sup>low</sup>  
387 monocytes. The inhibitory receptor hFc $\gamma$ RIIB was also significantly reduced on Ly6C<sup>hi</sup>  
388 monocytes, yet unchanged on Ly6C<sup>low</sup> monocytes and neutrophils. These changes in  
389 receptor staining were not due merely to increased quantities of circulating IgG, as the  
390 injection of non-aggregated IVIG did not affect receptor expression (Figure 5A-C).  
391 Receptor detection by anti-hFc $\gamma$ R mAbs may be influenced by pre-bound human IgG-  
392 immune complexes; however we confirmed that this was not the case using a panel of  
393 different antibodies with different recognition sites, both within and outside of the  
394 ligand-binding region. Furthermore, hIgG could be detected at low amounts on the  
395 surface of VG1543 neutrophils and monocytes isolated after IVIG-PSA (Supplementary

396 Figure 7 and Supplementary Methods), yet the limited amount of bound hIgG that we  
397 observe after PSA, particularly on neutrophils, certainly does not account for the several  
398 logs of reduction in receptor staining intensity. These data indicate active engagement  
399 of hFc $\gamma$ R on neutrophils and monocytes during IVIG-PSA, and suggest that these cells  
400 are each involved in responding to IgG-immune complexes, even though, in the case of  
401 monocytes, they may not be required for the induction of anaphylactic symptoms in  
402 VG1543 mice.

403

#### 404 **PAF and histamine contribute to IVIG-PSA in VG1543 mice**

405 We assessed the contribution of the mediators PAF and histamine to IVIG-PSA  
406 in VG1543 mice, using receptor antagonists administered before PSA induction. PAF  
407 receptor blockade using two different antagonists (ABT-491 and CV-6209) significantly  
408 reduced the hypothermia associated with IVIG-PSA in VG1543 mice (Figure 6A-B).  
409 Cetirizine, Pyrilamine and Tropolidine are different histamine-receptor 1 antagonists  
410 that inhibit IgE-induced PSA to various extents (Supplemental Figure 8A-C). Cetirizine  
411 had no effect on IVIG PSA in VG1543 mice, unless combined with PAF-R antagonist  
412 ABT-491 (Supplemental Figures 8D-E). Pyrilamine and Tropolidine, however,  
413 significantly reduced the hypothermia associated with IVIG-PSA in VG1543 mice  
414 (Figure 6C-D). Of note, PAF-R antagonist ABT-491 injected at higher doses did not  
415 confer greater protection (Supplemental Figure 8F). Therefore both PAF and histamine  
416 contribute to IVIG-PSA, in agreement with the contribution of neutrophils and  
417 basophils, in knock-in mice expressing human low-affinity IgG receptors.

418

419

**DISCUSSION**

420

421 We demonstrate here that VG1543 mice, which exhibit genuine expression of all  
422 human low-affinity Fc $\gamma$ R<sub>s</sub>, are susceptible to IgG-dependant anaphylaxis. VG1543, but  
423 not VG1505, mice experienced severe hypothermia following transfer of aggregated  
424 human IgG or following immunisation and challenge with the same antigen. These data  
425 show for the first time that, in a cognate context of activating and inhibitory human  
426 Fc $\gamma$ R signalling, immune complexes formed by either mouse or human IgG can trigger  
427 cell activation, mediator release, and severe anaphylaxis.

428

429 Several transgenic mouse models have been developed previously to investigate  
430 the *in vivo* functions of human Fc $\gamma$ R<sub>s</sub> (reviewed in <sup>14, 35</sup>). Transgenic approaches have  
431 their inherent flaws, however, in terms of reproducibility of human Fc $\gamma$ R expression,  
432 heterogeneity of transgene expression between individuals of the same genotype, and  
433 instability between generations, as a result of random transgene integration into the  
434 genome. hFc $\gamma$ RIIA(R<sub>131</sub>)<sup>tg</sup> mice<sup>41</sup>, hFc $\gamma$ RIIB(I<sub>232</sub>)<sup>tg</sup> <sup>42</sup>, hFc $\gamma$ RIIIA(F<sub>158</sub>)<sup>tg</sup> and  
435 hFc $\gamma$ RIIB<sup>tg</sup> (unknown polymorphic variant)<sup>43</sup> mice each employ their respective  
436 genuine human promoter to drive transgene expression. Of these, it appears that only  
437 hFc $\gamma$ RIIA(R<sub>131</sub>)<sup>tg</sup> mice recapitulate the corresponding human expression patterns<sup>28, 41</sup>,  
438 whereas hFc $\gamma$ RIIB(I<sub>232</sub>)<sup>tg</sup> mice exhibit abnormally high expression on circulating  
439 monocytes and granulocytes, and hFc $\gamma$ RIIIA(F<sub>158</sub>)<sup>tg</sup> hFc $\gamma$ RIIB<sup>tg</sup> mice have aberrant  
440 expression on DCs and eosinophils<sup>29, 42</sup>. Furthermore, the study of hFc $\gamma$ R-transgenic  
441 strains necessitates genetic backgrounds lacking endogenous mFc $\gamma$ R<sub>s</sub>, because mouse  
442 and human Fc $\gamma$ R<sub>s</sub> cross-bind human and mouse IgG, respectively (Table 1). hFc $\gamma$ R-  
443 transgenic mice have been studied on a background deficient in the FcR  $\gamma$ -chain

444 signalling subunit (FcR $\gamma$ <sup>KO</sup>), that lacks functional expression of mFc $\gamma$ RI, mFc $\gamma$ RIII,  
445 mFc $\gamma$ RIV and mFc $\epsilon$ RI<sup>44</sup>. Unfortunately FcR $\gamma$ <sup>KO</sup> mice have deficiencies in signalling  
446 through several non-FcR molecules, including integrin, cytokine and growth factor  
447 receptors, affecting leukocyte recruitment and vascular haemostasis; and these mice  
448 maintain inhibitory mFc $\gamma$ RIIB expression that can modulate hFc $\gamma$ R-induced signalling<sup>35</sup>,  
449 <sup>45-47</sup>. A mFc $\gamma$ R<sup>null</sup> background, lacking all mouse IgG receptor expression but  
450 maintaining FcR  $\gamma$ -chain expression, is a preferable approach, as exemplified in the  
451 generation of hFc $\gamma$ RI<sup>tg</sup>IIA<sup>tg</sup>IIB<sup>tg</sup>IIIA<sup>tg</sup>IIIB<sup>tg</sup> mFc $\gamma$ R<sup>null</sup> mice by intercrossing of the five  
452 single hFc $\gamma$ R-transgenic strains described above<sup>29</sup>.

453

454 To circumvent the inherent issues of randomly integrated transgenics, we  
455 employed gene knock-in technology to generate a mouse model deficient for the low-  
456 affinity mouse IgG receptor locus (mFc $\gamma$ RIIB/III/IV<sup>KO</sup>; VG1505), and to insert the  
457 human low-affinity IgG receptor locus in its stead (hFc $\gamma$ RIIA(H<sub>131</sub>)-hFc $\gamma$ RIIB(I<sub>232</sub>)-  
458 hFc $\gamma$ RIIC(Stop<sub>13</sub>)-hFc $\gamma$ RIIIA(V<sub>158</sub>)-hFc $\gamma$ RIIIB(NA2)<sup>KI</sup>; VG1543). Consequently,  
459 VG1543 mice demonstrate hFc $\gamma$ R expression consistent with that observed in humans<sup>26</sup>,  
460 <sup>35</sup>, with some minor differences: eosinophils lack hFc $\gamma$ RIIIA expression and basophils  
461 lack hFc $\gamma$ RIIB expression. In addition, hFc $\gamma$ RIIIA and hFc $\gamma$ RIIB expression is higher  
462 on blood monocytes compared to humans; nevertheless hFc $\gamma$ RIIB on these cells in  
463 VG1543 remains very much closer to that observed in humans, when compared to the  
464 expression reported in hFc $\gamma$ RI<sup>tg</sup>IIA<sup>tg</sup>IIB<sup>tg</sup>IIIA<sup>tg</sup>IIIB<sup>tg</sup> mFc $\gamma$ R<sup>null</sup> mice<sup>29</sup>. Of note, VG1543  
465 represent the first mouse model of hFc $\gamma$ RIIA(H<sub>131</sub>) and hFc $\gamma$ RIIIA(V<sub>158</sub>) expression,  
466 which is particularly advantageous for the study of human IgG2. Indeed hFc $\gamma$ RIIA(H<sub>131</sub>)  
467 binds significantly better human IgG2 than the polymorphic variant hFc $\gamma$ RIIA(R<sub>131</sub>),  
468 which is expressed in hFc $\gamma$ RIIA transgenic animals<sup>38, 48</sup>; and hFc $\gamma$ RIIIA(V<sub>158</sub>) binds

469 human IgG2 whereas polymorphic variant hFcγRIIIA(F<sub>158</sub>), expressed in hFcγRIIIA<sup>tg</sup>  
470 mice, does not<sup>38, 43, 48</sup>.

471 Here we identify for the first time that, within the context of native co-  
472 expression with other activating and inhibitory hFcγRs, hFcγRIIA drives IgG-  
473 anaphylaxis induction. hFcγRIIA blockade indeed protected VG1543 mice against  
474 systemic anaphylaxis induced by aggregated human IVIG. The transfer of IVIG  
475 aggregated *ex vivo* mimics the formation of polyclonal hIgG immune complexes *in vivo*,  
476 since the subclass composition reflects that of human serum: 63% IgG1, 29% IgG2, 5%  
477 IgG3 and 3% IgG4. All human FcγRs expressed in VG1543 mice bind human IgG1 and  
478 IgG3, only hFcγRIIA(H<sub>131</sub>) and hFcγRIIIA(V<sub>158</sub>) bind human IgG2, and all except  
479 hFcγRIIIB(NA2) bind human IgG4. Yet hFcγRIIA(H<sub>131</sub>) binds IgG2 with >7-fold  
480 higher affinity than hFcγRIIIA(V<sub>158</sub>)<sup>38</sup>, and therefore the IgG2 component of aggregated  
481 IVIG may bias towards hFcγRIIA(H<sub>131</sub>) engagement over the other hFcγRs expressed in  
482 VG1543 mice. hFcγRIIA blockade also protected VG1543 mice from systemic  
483 anaphylaxis and death following immunisation and challenge with the same antigen.  
484 This is a less physiological model, as it relies on human hFcγRs cross-binding mouse  
485 IgGs. Among the activating receptors expressed in VG1543 mice, only hFcγRIIA binds  
486 mouse IgG1 (Table 1) - the predominant IgG isotype produced during ASA  
487 immunisation - and logically therefore predominantly contributes to anaphylaxis  
488 induction.

489 While the protective effect of hFcγRIIA blockade in IVIG-PSA suggests that  
490 hFcγRIIIA and hFcγRIIIB are not individually capable of triggering systemic  
491 anaphylaxis, we cannot formally exclude a cooperative role of these receptors in  
492 anaphylaxis induction via hFcγRIIA in VG1543 mice. Indeed, we could not efficiently



493 block hFcγRIIIA and/or hFcγRIIIB *in vivo* using available anti-hFcγRIII antibodies  
494 (data not shown). We did observe significant hFcγRIIIA/B down-regulation on  
495 circulating neutrophils and monocytes after IVIG-PSA, but not after injection of non-  
496 aggregated IVIG (Figure 6), supporting the notion that these receptors are actively  
497 engaging with IgG immune complexes, despite not triggering a systemic reaction.  
498 Indeed, in models of autoantibody-induced inflammation, hFcγRIIA and hFcγRIIIB  
499 expressed on neutrophils were found to individually and cooperatively promote immune  
500 complex-induced reactions; however hFcγRIIA alone promoted associated injury and  
501 inflammation, whereas hFcγRIIIB rather mediated homeostatic clearance of immune  
502 complexes<sup>39, 49</sup>, suggesting that hFcγRIIA, but not hFcγRIIIB, is able to induce  
503 detrimental reactions *in vivo*. Anaphylaxis induced by aggregated IVIG was also  
504 demonstrated in the hFcγRI<sup>tg</sup>IIA<sup>tg</sup>IIB<sup>tg</sup>IIIA<sup>tg</sup>IIB<sup>tg</sup> mFcγR<sup>null</sup> mouse model<sup>29</sup>, but the  
505 contributing hFcγRs were not identified.

506

507       Importantly, VG1505 and VG1543 mice still express the high-affinity mouse  
508 receptor mFcγRI, which is expressed on monocytes, tissue resident monocyte-derived  
509 cells and specific macrophage populations<sup>26, 50, 51</sup> (Supplementary Figure 1). Even so,  
510 VG1505 mice were resistant to IVIG-PSA (and active anaphylaxis) induction,  
511 demonstrating that mFcγRI alone cannot trigger anaphylaxis, and that anaphylactic  
512 reactions in VG1543 mice rely exclusively on hFcγR triggering. We previously reported  
513 that the human counterpart of mFcγRI, hFcγRI (CD64) was sufficient to induce  
514 systemic anaphylaxis in transgenic mice lacking mouse FcγRs<sup>27</sup>. We used for this  
515 former study the only reported hFcγRI-transgenic mouse: it expresses this receptor on  
516 monocytes and macrophages as in humans, but also constitutively on neutrophils,  
517 contrarily to humans<sup>35, 52</sup>. Anaphylaxis in these mice relied on both neutrophils and

518 monocytes/macrophages<sup>27</sup>. Human Fc $\gamma$ RI is not expressed in the VG1543 background,  
519 and the question remains open whether hFc $\gamma$ RI can participate in IgG-induced  
520 anaphylaxis in a context of native hFc $\gamma$ R expression. We have developed a novel  
521 hFc $\gamma$ RI knock-in mouse strain that does not present the discrepant expression of  
522 existing hFc $\gamma$ RI-transgenic models<sup>29, 52</sup>: hFc $\gamma$ RI is expressed on monocytes,  
523 macrophages and dendritic cells, but not constitutively on neutrophils (data not shown).  
524 We are currently crossing this mouse strain to VG1543 mice, to create a fully hFc $\gamma$ R-  
525 humanized knock-in mouse model, which should enable us in the future to address the  
526 relative contribution of hFc $\gamma$ RI in a model recapitulating all hFc $\gamma$ R expression.

527

528 Anaphylaxis is driven by the release of anaphylactogenic mediators from  
529 myeloid cells<sup>4, 53</sup>. The contribution of any given cell population is therefore determined  
530 by the requisite expression of activating Fc $\gamma$ R, the capacity of the cells to release active  
531 mediators, and a cells' potential for negative inhibition of Fc $\gamma$ R signalling by expression  
532 of inhibitory Fc $\gamma$ RIIB<sup>54</sup>. In wild-type (wt) mice, pathways of active systemic  
533 anaphylaxis and passive IgG anaphylaxis rely predominantly on monocyte and/or  
534 neutrophil activation via mFc $\gamma$ RIII, with a minor contribution of mFc $\gamma$ RIV, and  
535 subsequent PAF release<sup>18, 19, 55</sup>. Considering genetic evolution, the functional homolog  
536 of mFc $\gamma$ RIII is hFc $\gamma$ RIIA, and that of mFc $\gamma$ RIV is hFc $\gamma$ RIIIA (H. Watier, personal  
537 communication)<sup>35</sup>. It is therefore consistent that hFc $\gamma$ RIIA, which exhibits prominent  
538 expression on all circulating myeloid cells, like mFc $\gamma$ RIII, may be the predominant IgG  
539 receptor contributing to anaphylaxis in VG1543 mice. We previously demonstrated that  
540 transgenic expression of hFc $\gamma$ RIIA(R<sub>131</sub>) was sufficient to induce passive active  
541 systemic anaphylaxis, and that IgG-induced PSA in hFc $\gamma$ RIIA(R<sub>131</sub>)<sup>tg</sup> mFc $\gamma$ RI/IIB/III<sup>KO</sup>  
542 mice required monocytes and neutrophils<sup>28</sup>.

543 Here, we identify that neutrophils are mandatory for anaphylaxis in VG1543  
544 mice, whereas we could not identify a contribution for monocytes/macrophages,  
545 although they express hFcγRIIA. This discrepancy between mouse models may be due  
546 to expression of inhibitory hFcγRIIB, absent in hFcγRIIA(R<sub>131</sub>)<sup>tg</sup> mFcγRI/IIB/III<sup>KO</sup> mice,  
547 but elevated on VG1543 blood monocytes compared to humans. Blood monocytes  
548 express consistently hFcγRIIB in VG1543 mice but we and others have identified  
549 variable hFcγRIIB on monocytes, particularly CD14<sup>lo</sup> blood monocytes, and prominent  
550 expression on only a fraction of human donors<sup>36</sup> (Supplementary Figure 2). Spleen  
551 monocytes, however, significantly express hFcγRIIB in humans<sup>36</sup> and VG1543 mice.  
552 Indeed, hFcγRIIB binds to all subclasses of human IgG<sup>38</sup> and therefore may inhibit  
553 monocyte activation following engagement by IVIG aggregates in VG1543 mice. On  
554 one hand, we observed down-regulation of inhibitory hFcγRIIB on circulating Ly6C<sup>hi</sup>  
555 and Ly6C<sup>low</sup> monocytes following IVIG-PSA suggesting its engagement by IVIG-  
556 immune complexes and potential inhibitory signalling by this receptor; on the other  
557 hand blockade of hFcγRIIB did not modulate anaphylactic symptoms in VG1543 mice.  
558 hFcγRIIB, and the inhibitory signals it can induce, do not appear to regulate this model  
559 of anaphylaxis. These data do not favour a contribution of monocytes to anaphylaxis in  
560 VG1543 mice. We cannot, however, exclude a potential contribution of blood  
561 monocytes (mostly hFcγRIIB negative) to human anaphylaxis.

562

563 The contribution of basophils to anaphylaxis models in mice remains  
564 controversial: mIgG1-induced PSA<sup>17</sup> and mIgG2a-induced PSA<sup>55</sup> were inhibited  
565 following antibody-mediated basophil depletion, but mIgG1-induced PSA was  
566 unaffected in Mcpt8-cre mice that exhibit >90% basophil deficiency<sup>56</sup>. In an active  
567 model of peanut-induced anaphylaxis, involving both IgE and IgG, both antibody- or

568 diphtheria toxin-mediated basophil depletion significantly reduced hypothermia<sup>57</sup>.  
569 Human basophils express variable levels of hFcγRIIA and high levels of hFcγRIIB, yet  
570 could not be activated by hIgG immune complexes *in vitro*, suggesting that hFcγRIIB-  
571 dependent negative regulation is dominant over hFcγRIIA-dependent basophil  
572 activation<sup>37</sup>. VG1543 mice express hFcγRIIA at low levels on circulating basophils, but  
573 within the range of that observed on peripheral blood cells from healthy donors (Figure  
574 2A-B). Unlike human basophils, however, VG1543 basophils do not express hFcγRIIB:  
575 that we do not identify a major contribution of basophils to anaphylaxis in VG1543  
576 mice cannot be due to hFcγRIIB inhibition of hFcγRIIA-mediated signalling.

577 We reported previously that neutrophils predominantly contribute to ASA in wt  
578 mice and that the transfer of human neutrophils can restore anaphylaxis in resistant  
579 mice<sup>13, 19</sup>. Neutrophils were mandatory for IVIG-PSA (and ASA) in VG1543 mice,  
580 since neutrophil depletion abolished hypothermia and protected from death. Both of  
581 these anaphylaxis models were dependent on hFcγRIIA, which is expressed at very high  
582 levels on both human and VG1543 mouse neutrophils, whereas inhibitory hFcγRIIB  
583 expression is found only on a small subset of neutrophils. This low or absent hFcγRIIB  
584 expression implies that, unlike monocytes, neutrophil activation is not, or marginally,  
585 regulated by inhibitory hFcγRIIB. Neutrophils also contributed to hFcγRIIA-dependent  
586 PSA in hFcγRIIA(R<sub>131</sub>)<sup>Ig</sup> mFcγRI/IIB/III<sup>KO</sup> mice<sup>28</sup> in the absence of other hFcγR  
587 expression. We demonstrate now that the contribution of neutrophils to IgG-induced  
588 anaphylaxis is also predominant in the context of native hFcγR expression in VG1543  
589 mice. Such an observation is of crucial consideration when we acknowledge that  
590 neutrophils comprise >60% of circulating blood cells in humans.

591

592 Finally, we identified that the soluble mediator PAF was responsible for a  
593 significant proportion of IVIG-PSA-induced hypothermia (and ASA-associated death),  
594 a finding concurrent with a dominant pathway initiated by hFcγRIIA on neutrophils.  
595 Neutrophils are indeed the major producers of PAF in humans<sup>58</sup>. Among the three  
596 Histamine receptor antagonists tested, two (Pyrilamine and Tripolidine) significantly  
597 inhibited IVIG-induced anaphylaxis by themselves, and one (Cetirizine) only had an  
598 effect when combined with PAF-R antagonists. These findings suggest that both PAF  
599 and histamine contribute to hypothermia and mortality in the VG1543 model. These  
600 results are in agreement with the inefficacy of H1-antihistamine treatment alone on  
601 systemic anaphylactic symptoms in patients. Reports by Vadas and colleagues indicate  
602 a correlation between levels of circulating PAF, rather than histamine, with anaphylaxis  
603 severity<sup>12</sup>, and identified PAF as a central mediator of human anaphylaxis  
604 pathogenesis<sup>59</sup>; which aligns with our findings reported herein using locus-swapped  
605 human low-affinity hFcγR<sup>KI</sup> mice.

606  
607 Our data indicate that IgG-dependant anaphylaxis in VG1543 mice proceeds via  
608 an activating pathway dependent on hFcγRIIA and neutrophils, with a contribution of  
609 basophils, and driven by the mediators PAF and histamine. Although expressed in this  
610 novel knock-in mouse model, hFcγRIIA and hFcγRIIIB were not sufficient to trigger  
611 anaphylaxis. That such drastic anaphylaxis induction is possible in the context of native  
612 inhibitory and activating hFcγR expression suggests a similar pathway may occur in  
613 humans. VG1543 mice represent an attractive knock-in model for the study of human  
614 low-affinity IgG receptors, in which the encoding genes remain expressed in their  
615 cognate genetic environment, including intergenic sequences; and consequently cell  
616 surface expression largely reflects that of humans. Although the polymorphisms

617 expressed in the VG1543 mouse represent a section of individuals within the population,  
618 other people express alternate and/or heterozygous polymorphisms, some of which have  
619 been demonstrated to predispose to immunological susceptibility or resistance<sup>14</sup>. It  
620 would be clinically relevant to extend studies in hFcγR-knock in mice to understand the  
621 effect of hFcγR polymorphisms on cell activation and subsequent biological responses,  
622 and therefore on sensitivity to anaphylaxis or other allergic diseases involving IgG  
623 antibodies.  
624

625

**ACKNOWLEDGMENTS**

626 We are thankful to O. Godon, B. Iannascoli and O. Richard-LeGoff for technical  
627 help, P. Vieira and L. Reber for scientific advice and D. Sinnaya for administrative help  
628 (Institut Pasteur, Paris). We are thankful to our colleagues for their generous gifts: R.  
629 Coffman (DNAX, Palo Alto, CA, USA), R. Good (USFCM, Tampa, FL, USA), H.  
630 Karasuyama (Tokyo Medical and Dental University Graduate School, Tokyo, Japan)  
631 and D. Voehringer (Universitätsklinikum, Erlangen, Germany) for antibodies. C12MDP  
632 was a gift of Roche Diagnostics GmbH. This work was supported by the European  
633 Research Council (ERC)–Seventh Frame-work Program (ERC-2013-CoG 616050);  
634 additional support by the Institut Pasteur and the Institut National de la Santé et de la  
635 Recherche Médicale (INSERM). C.G. was supported partly by a stipend from the  
636 Pasteur - Paris University (PPU) International PhD program and by the Institut Carnot  
637 Pasteur Maladies Infectieuses, and partly by the Balsan company. F.J. is an employee of  
638 the Centre National de La Recherche Scientifique (CNRS). H.B. is supported by a  
639 fellowship from the University Pierre et Marie Curie.

640

**AUTHORSHIP AND CONFLICT OF INTEREST STATEMENTS**

642 C.G. performed all experiments, with contributions from F.J., D.A.M. and H.B.;  
643 A.M., L.E.M. and N.T. designed mouse targeting and generated mouse strains; N.v.R.  
644 provided reagents; C.G., F.J., L.E.M. and P.B. analysed and discussed results; C.G. and  
645 P.B. wrote the manuscript; P.B. supervised and designed the research.

646 LM, NT and AM are employees of Regeneron Pharmaceuticals, Inc. and hold stock in  
647 the company. H.B., P.B, C.G., B.I., F.J. and D.A.M. declare no competing financial  
648 interests.

649

650

**FIGURE LEGENDS**

651

652 **Figure 1: Humanization of the mouse low-affinity receptor locus.** Representations  
653 are not drawn to scale. (A) Deletion of mouse *Fcgr2b*, *Fcgr4* and *Fcgr3* genes in a single  
654 targeting step, deleting mouse sequences from 1:170,956,770 to 1:171,063,353 on  
655 mouse Chr1\_H3 (based on mouse GRCh38). (B) Insertion of human FCGR3A and  
656 FCGR2A genes and (C) insertion of FCGR2B, FCGR3B and FCGR2C genes. The total  
657 human sequence inserted in VG1543 ranges from 1:161,500,441 to 1:161,679,348 on  
658 human Chr1\_q23.3, based on human GRCh38. Mouse genomic coordinates are in black,  
659 human genomic coordinates are in grey, light grey block arrow indicates Hygromycin  
660 selection cassettes, dark grey block arrows indicate Neomycin selection cassettes, black  
661 triangles represent *Loxp* sites, empty triangles represent *Frt* sites and grey triangles  
662 represent *Lox2372* sites.

663

664 **Figure 2: Human FcγR expression on immune cell populations from VG1543 mice**  
665 **recapitulates expression patterns in humans**

666 (A) hFcγRIIA, hFcγRIIB, hFcγRIIIA and hFcγRIIIB staining on immune cells from  
667 human peripheral blood, assessed by fluorescent antibody labelling and flow cytometric  
668 analysis. Shaded histograms indicate staining with an isotype control antibody,  
669 excepting hFcγRIIB where shaded histograms indicate a fluorescence-minus-one  
670 (FMO) control. (B) hFcγR staining on immune cells isolated from different tissues of  
671 VG1543 mice, as indicated. Shaded histograms indicate background staining from  
672 VG1505 mice. Data are representative of at least 2 independent experiments; total n>3.  
673 BAL: bronchoalveolar lavage. Numbers indicate frequency of cells positive for FcγR



674 staining. (C) Individual variation in hFcγRIIA expression on basophils isolated from 4  
675 different blood donors (upper panels) or from 4 different 1543 mice (lower panels).

676

677 **Figure 3: VG1543 mice are susceptible to active systemic anaphylaxis, dominantly**  
678 **mediated by hFcγRIIA, neutrophils and PAF.**

679 Indicated mice were immunised and challenged with BSA, and central temperatures and  
680 survival rates were monitored. (A) Change in body temperature (upper panel) and  
681 survival (lower panel) during BSA-ASA in VG1505 (crossed circles) and VG1543  
682 (squares) mice. (B-D) BSA-ASA in VG1505 and VG1543 mice, and VG1543 mice  
683 treated with (B) anti-hFcγRIIA blocking mAbs or isotype control, (C) anti-Ly6G mAbs  
684 or isotype control, (D) vehicle (NaCl) or PAF-R antagonist ABT-491. Data are  
685 represented as mean ± SEM and are representative of at least 2 independent experiments.  
686 Numbers indicate mortality per experimental group; X represents 100% mortality. (#  
687 p<0.05 ; ### p<0.001, Log-rank (Mantel-Cox) test for survival; \* p<0.05, \*\* p<0.01,  
688 Student's t-test of individual time points from 10 to 40min)

689

690 **Figure 4: Aggregated human IVIG triggers passive systemic anaphylaxis in**  
691 **VG1543 mice, mediated by hFcγRIIA and neutrophils.**

692 VG1505 (circles) and VG1543 (squares) mice were injected with (A) 1mg or (B)  
693 indicated amounts of heat-aggregated IVIG and central temperatures monitored. (C-F)  
694 IVIG-PSA (1mg) in VG1543 mice injected with (C) anti-hFcγRIIA blocking mAbs, (D)  
695 toxin-containing liposomes, (E) anti-CD200R3 mAbs, (F) anti-Ly6G mAbs, or  
696 corresponding isotype or PBS controls, prior to anaphylaxis induction. (G) IVIG-PSA  
697 (250μg) in VG1543 mice injected with indicated amounts of anti-hFcγRIIB blocking  
698 mAbs. White or grey squares indicate treated mice; black squares indicate isotype or

699 vehicle controls. (A-F) Data are represented as mean  $\pm$  SEM and are representative of at  
700 least 2 independent experiments. (G) Data are represented as mean values of  
701 independent experiments. (\* $p$ <0.05, \*\* $p$ <0.01; 2-way RM-ANOVA).

702

703 **Figure 5: Reduction in hFc $\gamma$ R expression on circulating myeloid cell populations**  
704 **after IVIG-PSA.** hFc $\gamma$ RIIA, hFc $\gamma$ RIIB and hFc $\gamma$ RIII expression on (A) blood  
705 neutrophils, (B) Ly6C<sup>hi</sup> and (C) Ly6C<sup>low</sup> monocytes from VG1543 mice; 1 hour after  
706 injection of vehicle (NaCl), non-aggregated IVIG (non-agg) or heat aggregated-IVIG  
707 and PSA induction (HA-IVIG). Background staining on cells from VG1505 mice is  
708 shown 1 hour after injection of heat aggregated-IVIG. Values represent  $\Delta$ GeoMean  
709 between specific staining and corresponding isotype or FMO control, pooled from three  
710 independent experiments. Representative histograms are shown in (D); background  
711 staining of isotype control is indicated by shaded histograms; VG1505 mice by grey  
712 histograms. (\*\* $p$ <0.001, \* $p$ <0.05, unpaired t test with Welch's correction)

713

714 **Figure 6: The anaphylactic mediators PAF and histamine are responsible for**  
715 **IVIG-PSA in VG1543 mice.** PSA was induced by 1mg heat-aggregated IVIG and  
716 central temperatures monitored: indicated mice were pre-treated, with PAF-R  
717 antagonists (A) ABT-491 or (B) CV-6209, H1-R antagonists (C) pyrilamine maleate or  
718 (D) triprolidine hydrochloride, or with vehicle (NaCl). Data are represented as mean  $\pm$   
719 SEM and are representative of at least 2 independent experiments (\* $p$ <0.05, \*\* $p$ <0.01,  
720 VG1543 treated vs controls, 2-way RM-ANOVA)

721

722

723

## TABLES

724

725 **Table 1:** Binding and crossbinding of human and mouse IgG subclasses to human and

726 mouse FcγRs

727 -, no binding; +/-, very-low binding; +, low-binding; ++, medium binding; +++, high

728 binding. Adapted from data reported in <sup>19, 38, 60, 61</sup> and unpublished data.

		HUMAN				MOUSE			
		IgG1	IgG2	IgG3	IgG4	IgG1	IgG2a/c	IgG2b	IgG3
HUMAN	<b>hFcγRI</b>	+++	-	+++	+++	-	+++	+++	+/-
	<b>hFcγRIIA(H131)</b>	++	+	+	+	+	+	+	-
	<b>hFcγRIIA(R131)</b>	++	+	+	+	++	+	+	-
	<b>hFcγRIIB</b>	+	+/-	+	+	-	-	+/-	-
	<b>hFcγRIIC</b>	+	+/-	+	+	-	-	+/-	-
	<b>hFcγRIIA(V158)</b>	+	+/-	+++	+	-	+/-	-	-
	<b>hFcγRIIA(F158)</b>	+	+/-	++	+	-	-	-	-
	<b>hFcγRIIB(NA1)</b>	+	-	++	-	-	-	-	-
	<b>hFcγRIIB(NA2)</b>	+	-	++	-	-	-	-	-
	<b>hFcγRIIB(SH)</b>	+	-	++	-	-	-	-	-
MOUSE	<b>mFcγRI</b>	+++	-	++	++	-	+++	+	+/-
	<b>mFcγRIIB</b>	-	+/-	-	-	++	+	++	-
	<b>mFcγRIII</b>	++	++	+/-	-	+	+	+	-
	<b>mFcγRIV</b>	++	+	++	+/-	-	+++	+++	-

729

730

## REFERENCES

- 731  
732  
733 1. Mullins RJ, Dear KB, Tang ML. Time trends in Australian hospital anaphylaxis  
734 admissions in 1998-1999 to 2011-2012. *J Allergy Clin Immunol* 2015; 136:367-  
735 75.
- 736 2. Nocerino R, Leone L, Cosenza L, Berni Canani R. Increasing rate of  
737 hospitalizations for food-induced anaphylaxis in Italian children: An analysis of  
738 the Italian Ministry of Health database. *J Allergy Clin Immunol* 2015; 135:833-5  
739 e3.
- 740 3. Turner PJ, Gowland MH, Sharma V, Ierodiakonou D, Harper N, Garcez T, et al.  
741 Increase in anaphylaxis-related hospitalizations but no increase in fatalities: an  
742 analysis of United Kingdom national anaphylaxis data, 1992-2012. *J Allergy*  
743 *Clin Immunol* 2015; 135:956-63 e1.
- 744 4. Lee JK, Vadas P. Anaphylaxis: mechanisms and management. *Clin Exp Allergy*  
745 2011; 41:923-38.
- 746 5. Fisher MM, Baldo BA. Mast cell tryptase in anaesthetic anaphylactoid reactions.  
747 *Br J Anaesth* 1998; 80:26-9.
- 748 6. Cheifetz A, Smedley M, Martin S, Reiter M, Leone G, Mayer L, et al. The  
749 incidence and management of infusion reactions to infliximab: a large center  
750 experience. *Am J Gastroenterol* 2003; 98:1315-24.
- 751 7. Dybendal T, Guttormsen AB, Elsayed S, Askeland B, Harboe T, Florvaag E.  
752 Screening for mast cell tryptase and serum IgE antibodies in 18 patients with  
753 anaphylactic shock during general anaesthesia. *Acta Anaesthesiol Scand* 2003;  
754 47:1211-8.
- 755 8. Golden DB. Patterns of anaphylaxis: acute and late phase features of allergic  
756 reactions. *Novartis Found Symp* 2004; 257:101-10; discussion 10-5, 57-60, 276-  
757 85.
- 758 9. Mertes PM, Alla F, Trechot P, Auroy Y, Jouglu E. Anaphylaxis during  
759 anesthesia in France: an 8-year national survey. *J Allergy Clin Immunol* 2011;  
760 128:366-73.
- 761 10. Laroche D, Gomis P, Gallimidi E, Malinovsky JM, Mertes PM. Diagnostic  
762 value of histamine and tryptase concentrations in severe anaphylaxis with shock  
763 or cardiac arrest during anesthesia. *Anesthesiology* 2014; 121:272-9.
- 764 11. Vadas P, Gold M, Perelman B, Liss GM, Lack G, Blyth T, et al. Platelet-  
765 activating factor, PAF acetylhydrolase, and severe anaphylaxis. *N Engl J Med*  
766 2008; 358:28-35.
- 767 12. Vadas P, Perelman B, Liss G. Platelet-activating factor, histamine, and tryptase  
768 levels in human anaphylaxis. *J Allergy Clin Immunol* 2013; 131:144-9.
- 769 13. Jonsson F, Mancardi DA, Albanesi M, Bruhns P. Neutrophils in local and  
770 systemic antibody-dependent inflammatory and anaphylactic reactions. *J Leukoc*  
771 *Biol* 2013; 94:643-56.
- 772 14. Gillis C, Gouel-Cheron A, Jonsson F, Bruhns P. Contribution of Human  
773 FcγR3s to Disease with Evidence from Human Polymorphisms and  
774 Transgenic Animal Studies. *Front Immunol* 2014; 5:254.
- 775 15. Oettgen HC, Martin TR, Wynshaw-Boris A, Deng C, Drazen JM, Leder P.  
776 Active anaphylaxis in IgE-deficient mice. *Nature* 1994; 370:367-70.
- 777 16. Miyajima I, Dombrowicz D, Martin TR, Ravetch JV, Kinet JP, Galli SJ.  
778 Systemic anaphylaxis in the mouse can be mediated largely through IgG1 and  
779 Fc γRIII. Assessment of the cardiopulmonary changes, mast cell

- 780 degranulation, and death associated with active or IgE- or IgG1-dependent  
781 passive anaphylaxis. *J Clin Invest* 1997; 99:901-14.
- 782 17. Tsujimura Y, Obata K, Mukai K, Shindou H, Yoshida M, Nishikado H, et al.  
783 Basophils play a pivotal role in immunoglobulin-G-mediated but not  
784 immunoglobulin-E-mediated systemic anaphylaxis. *Immunity* 2008; 28:581-9.
- 785 18. Strait RT, Morris SC, Yang M, Qu XW, Finkelman FD. Pathways of  
786 anaphylaxis in the mouse. *J Allergy Clin Immunol* 2002; 109:658-68.
- 787 19. Jönsson F, Mancardi DA, Kita Y, Karasuyama H, Iannascoli B, Van Rooijen N,  
788 et al. Mouse and human neutrophils induce anaphylaxis. *J Clin Invest* 2011;  
789 121:1484-96.
- 790 20. Iff ET, Vaz NM. Mechanisms of anaphylaxis in the mouse. Similarity of shock  
791 induced by anaphylaxis and by mixtures of histamine and serotonin. *Int Arch*  
792 *Allergy Appl Immunol* 1966; 30:313-22.
- 793 21. Million M, Fioramonti J, Zajac JM, Bueno L. Effects of neuropeptide FF on  
794 intestinal motility and temperature changes induced by endotoxin and platelet-  
795 activating factor. *Eur J Pharmacol* 1997; 334:67-73.
- 796 22. van de Veen W, Stanic B, Yaman G, Wawrzyniak M, Sollner S, Akdis DG, et al.  
797 IgG4 production is confined to human IL-10-producing regulatory B cells that  
798 suppress antigen-specific immune responses. *J Allergy Clin Immunol* 2013;  
799 131:1204-12.
- 800 23. Rispens T, Derksen NI, Commins SP, Platts-Mills TA, Aalberse RC. IgE  
801 production to alpha-gal is accompanied by elevated levels of specific IgG1  
802 antibodies and low amounts of IgE to blood group B. *PLoS One* 2013; 8:e55566.
- 803 24. Patil SU, Ogunniyi AO, Calatroni A, Tadigotla VR, Ruitter B, Ma A, et al.  
804 Peanut oral immunotherapy transiently expands circulating Ara h 2-specific B  
805 cells with a homologous repertoire in unrelated subjects. *J Allergy Clin*  
806 *Immunol* 2015; 136:125-34 e12.
- 807 25. Hoh RA, Joshi SA, Liu Y, Wang C, Roskin KM, Lee JY, et al. Single B-cell  
808 deconvolution of peanut-specific antibody responses in allergic patients. *J*  
809 *Allergy Clin Immunol* 2015.
- 810 26. Bruhns P. Properties of mouse and human IgG receptors and their contribution  
811 to disease models. *Blood* 2012; 119:5640-9.
- 812 27. Mancardi DA, Albanesi M, Jonsson F, Iannascoli B, Van Rooijen N, Kang X, et  
813 al. The high-affinity human IgG receptor FcγRI (CD64) promotes IgG-  
814 mediated inflammation, anaphylaxis, and antitumor immunotherapy. *Blood*  
815 2013; 121:1563-73.
- 816 28. Jönsson F, Mancardi DA, Zhao W, Kita Y, Iannascoli B, Khun H, et al. Human  
817 FcγRIIA induces anaphylactic and allergic reactions. *Blood* 2012;  
818 119:2533-44.
- 819 29. Smith P, DiLillo DJ, Bournazos S, Li F, Ravetch JV. Mouse model  
820 recapitulating human Fcγ receptor structural and functional diversity. *Proc*  
821 *Natl Acad Sci U S A* 2012; 109:6181-6.
- 822 30. Meyer T, Robles-Carrillo L, Davila M, Brodie M, Desai H, Rivera-Amaya M, et  
823 al. CD32a antibodies induce thrombocytopenia and type II hypersensitivity  
824 reactions in FCGR2A mice. *Blood* 2015; 126:2230-8.
- 825 31. Valenzuela DM, Murphy AJ, Friendewey D, Gale NW, Economides AN,  
826 Auerbach W, et al. High-throughput engineering of the mouse genome coupled  
827 with high-resolution expression analysis. *Nat Biotechnol* 2003; 21:652-9.

- 828 32. Macdonald LE, Karow M, Stevens S, Auerbach W, Poueymirou WT, Yasenchak  
829 J, et al. Precise and in situ genetic humanization of 6 Mb of mouse  
830 immunoglobulin genes. *Proc Natl Acad Sci U S A* 2014; 111:5147-52.
- 831 33. Auerbach W, Dunmore JH, Fairchild-Huntress V, Fang Q, Auerbach AB,  
832 Huszar D, et al. Establishment and chimera analysis of 129/SvEv- and  
833 C57BL/6-derived mouse embryonic stem cell lines. *Biotechniques* 2000;  
834 29:1024-8, 30, 32.
- 835 34. Veri MC, Gorlatov S, Li H, Burke S, Johnson S, Stavenhagen J, et al.  
836 Monoclonal antibodies capable of discriminating the human inhibitory  
837 Fc $\gamma$ -receptor IIB (CD32B) from the activating Fc $\gamma$ -receptor IIA  
838 (CD32A): biochemical, biological and functional characterization. *Immunology*  
839 2007; 121:392-404.
- 840 35. Bruhns P, Jonsson F. Mouse and human FcR effector functions. *Immunol Rev*  
841 2015; 268:25-51.
- 842 36. Tutt AL, James S, Laversin SA, Tipton TR, Ashton-Key M, French RR, et al.  
843 Development and Characterization of Monoclonal Antibodies Specific for  
844 Mouse and Human Fc $\gamma$  Receptors. *J Immunol* 2015; 195:5503-16.
- 845 37. Cassard L, Jonsson F, Arnaud S, Daeron M. Fc $\gamma$  receptors inhibit mouse  
846 and human basophil activation. *J Immunol* 2012; 189:2995-3006.
- 847 38. Bruhns P, Iannascoli B, England P, Mancardi DA, Fernandez N, Jorieux S, et al.  
848 Specificity and affinity of human Fc $\gamma$  receptors and their polymorphic  
849 variants for human IgG subclasses. *Blood* 2009; 113:3716-25.
- 850 39. Tsuboi N, Asano K, Lauterbach M, Mayadas TN. Human neutrophil Fc $\gamma$   
851 receptors initiate and play specialized nonredundant roles in antibody-mediated  
852 inflammatory diseases. *Immunity* 2008; 28:833-46.
- 853 40. Khodoun MV, Strait R, Armstrong L, Yanase N, Finkelman FD. Identification  
854 of markers that distinguish IgE- from IgG-mediated anaphylaxis. *Proc Natl Acad*  
855 *Sci U S A* 2011; 108:12413-8.
- 856 41. McKenzie SE, Taylor SM, Malladi P, Yuhan H, Cassel DL, Chien P, et al. The  
857 role of the human Fc receptor Fc  $\gamma$  RIIA in the immune clearance of  
858 platelets: a transgenic mouse model. *J Immunol* 1999; 162:4311-8.
- 859 42. Li F, Ravetch JV. Inhibitory Fc $\gamma$  receptor engagement drives adjuvant and  
860 anti-tumor activities of agonistic CD40 antibodies. *Science* 2011; 333:1030-4.
- 861 43. Li M, Wirthmueller U, Ravetch JV. Reconstitution of human Fc  $\gamma$  RIII  
862 cell type specificity in transgenic mice. *J Exp Med* 1996; 183:1259-63.
- 863 44. Takai T, Li M, Sylvestre D, Clynes R, Ravetch JV. FcR  $\gamma$  chain deletion  
864 results in pleiotropic effector cell defects. *Cell* 1994; 76:519-29.
- 865 45. Borges L, Cosman D. LIRs/ILTs/MIRs, inhibitory and stimulatory Ig-  
866 superfamily receptors expressed in myeloid and lymphoid cells. *Cytokine*  
867 *Growth Factor Rev* 2000; 11:209-17.
- 868 46. Zarbock A, Abram CL, Hundt M, Altman A, Lowell CA, Ley K. PSGL-1  
869 engagement by E-selectin signals through Src kinase Fgr and ITAM adapters  
870 DAP12 and FcR  $\gamma$  to induce slow leukocyte rolling. *J Exp Med* 2008;  
871 205:2339-47.
- 872 47. Boulaftali Y, Hess PR, Kahn ML, Bergmeier W. Platelet immunoreceptor  
873 tyrosine-based activation motif (ITAM) signaling and vascular integrity. *Circ*  
874 *Res* 2014; 114:1174-84.
- 875 48. Warmerdam PA, van de Winkel JG, Gosselin EJ, Capel PJ. Molecular basis for  
876 a polymorphism of human Fc  $\gamma$  receptor II (CD32). *J Exp Med* 1990;  
877 172:19-25.

- 878 49. Chen K, Nishi H, Travers R, Tsuboi N, Martinod K, Wagner DD, et al.  
879 Endocytosis of soluble immune complexes leads to their clearance by  
880 FcγRIIIB but induces neutrophil extracellular traps via FcγRIIA in  
881 vivo. *Blood* 2012; 120:4421-31.
- 882 50. Mancardi DA, Jonsson F, Iannascoli B, Khun H, Van Rooijen N, Huerre M, et al.  
883 The murine high-affinity IgG receptor Fc(γ)RIV is sufficient for  
884 autoantibody-induced arthritis. *J Immunol* 2011; 186:1899-903.
- 885 51. Langlet C, Tamoutounour S, Henri S, Luche H, Ardouin L, Gregoire C, et al.  
886 CD64 Expression Distinguishes Monocyte-Derived and Conventional Dendritic  
887 Cells and Reveals Their Distinct Role during Intramuscular Immunization. *J*  
888 *Immunol* 2012; 188:1751-60.
- 889 52. Heijnen IA, van Vugt MJ, Fanger NA, Graziano RF, de Wit TP, Hofhuis FM, et  
890 al. Antigen targeting to myeloid-specific human Fc γRI/CD64 triggers  
891 enhanced antibody responses in transgenic mice. *J Clin Invest* 1996; 97:331-8.
- 892 53. Brown SG, Stone SF, Fatovich DM, Burrows SA, Holdgate A, Celenza A, et al.  
893 Anaphylaxis: Clinical patterns, mediator release, and severity. *J Allergy Clin*  
894 *Immunol* 2013.
- 895 54. Smith KG, Clatworthy MR. FcγRIIIB in autoimmunity and infection:  
896 evolutionary and therapeutic implications. *Nat Rev Immunol* 2010; 10:328-43.
- 897 55. Khoudoun MV, Kucuk ZY, Strait RT, Krishnamurthy D, Janek K, Clay CD, et al.  
898 Rapid desensitization of mice with anti-FcγRIIb/FcγRIII mAb  
899 safely prevents IgG-mediated anaphylaxis. *J Allergy Clin Immunol* 2013;  
900 132:1375-87.
- 901 56. Ohnmacht C, Schwartz C, Panzer M, Schiedewitz I, Naumann R, Voehringer D.  
902 Basophils orchestrate chronic allergic dermatitis and protective immunity  
903 against helminths. *Immunity* 2010; 33:364-74.
- 904 57. Reber LL, Marichal T, Mukai K, Kita Y, Tokuoka SM, Roers A, et al. Selective  
905 ablation of mast cells or basophils reduces peanut-induced anaphylaxis in mice.  
906 *J Allergy Clin Immunol* 2013; 132:881-8 e11.
- 907 58. Jouvin-Marche E, Ninio E, Beaurain G, Tence M, Niaudet P, Benveniste J.  
908 Biosynthesis of Paf-acether (platelet-activating factor). VII. Precursors of Paf-  
909 acether and acetyl-transferase activity in human leukocytes. *J Immunol* 1984;  
910 133:892-8.
- 911 59. Gill P, Jindal NL, Jagdis A, Vadas P. Platelets in the immune response:  
912 Revisiting platelet-activating factor in anaphylaxis. *J Allergy Clin Immunol*  
913 2015; 135:1424-32.
- 914 60. Nimmerjahn F, Bruhns P, Horiuchi K, Ravetch JV. Fc γRIV: a novel FcR  
915 with distinct IgG subclass specificity. *Immunity* 2005; 23:41-51.
- 916 61. Mancardi DA, Iannascoli B, Hoos S, England P, Daeron M, Bruhns P.  
917 FcγRIV is a mouse IgE receptor that resembles macrophage FcεRI  
918 in humans and promotes IgE-induced lung inflammation. *J Clin Invest* 2008;  
919 118:3738-50.  
920

Figure 1

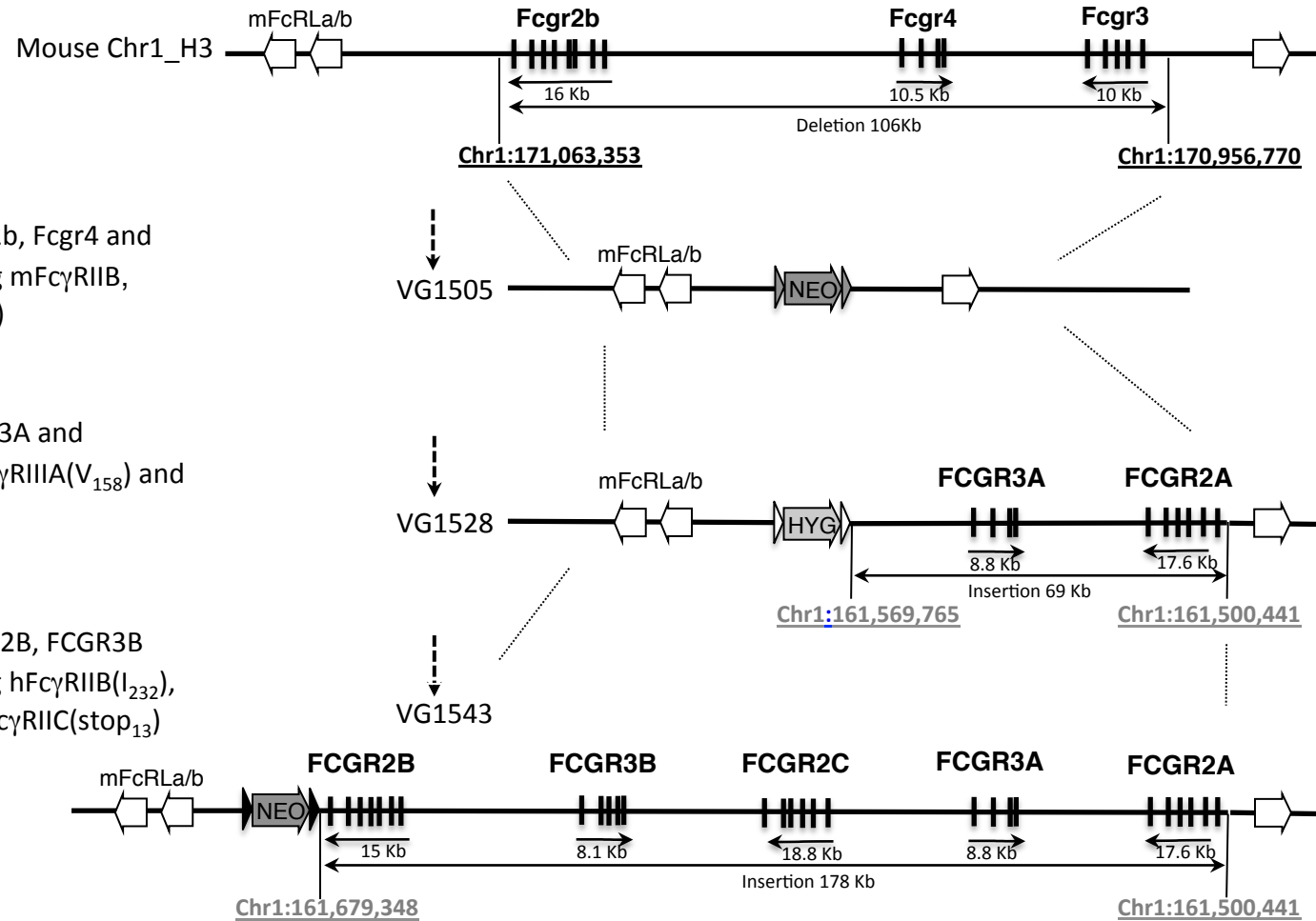
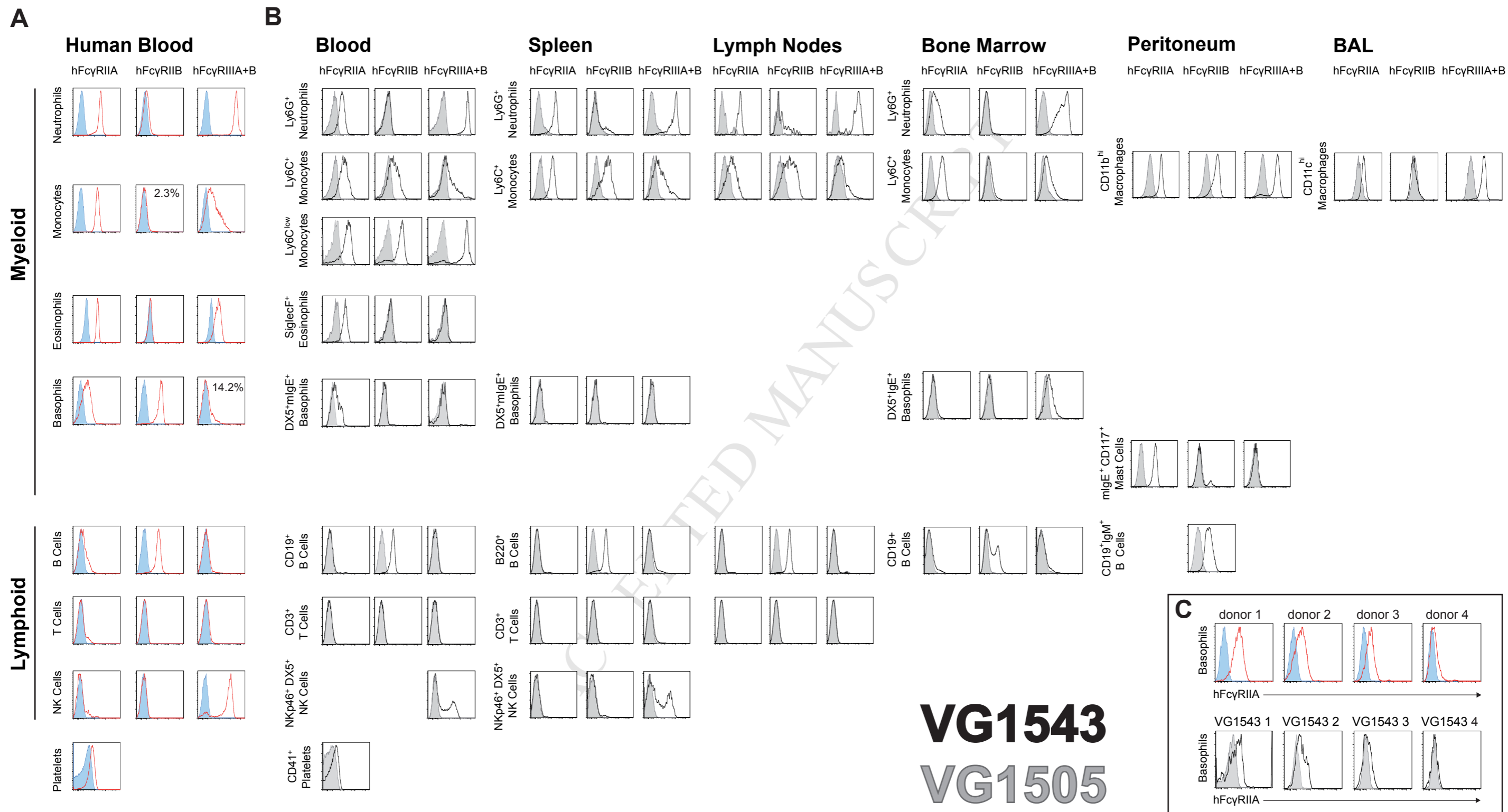




Figure 2



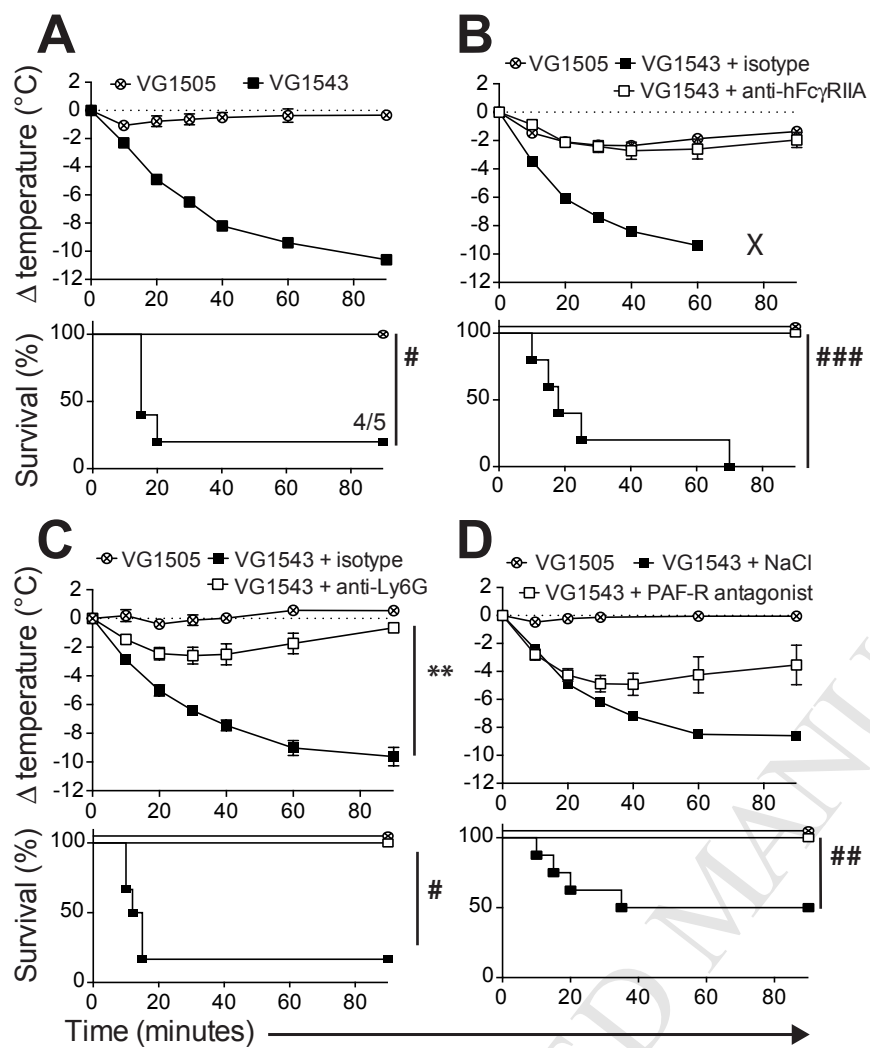
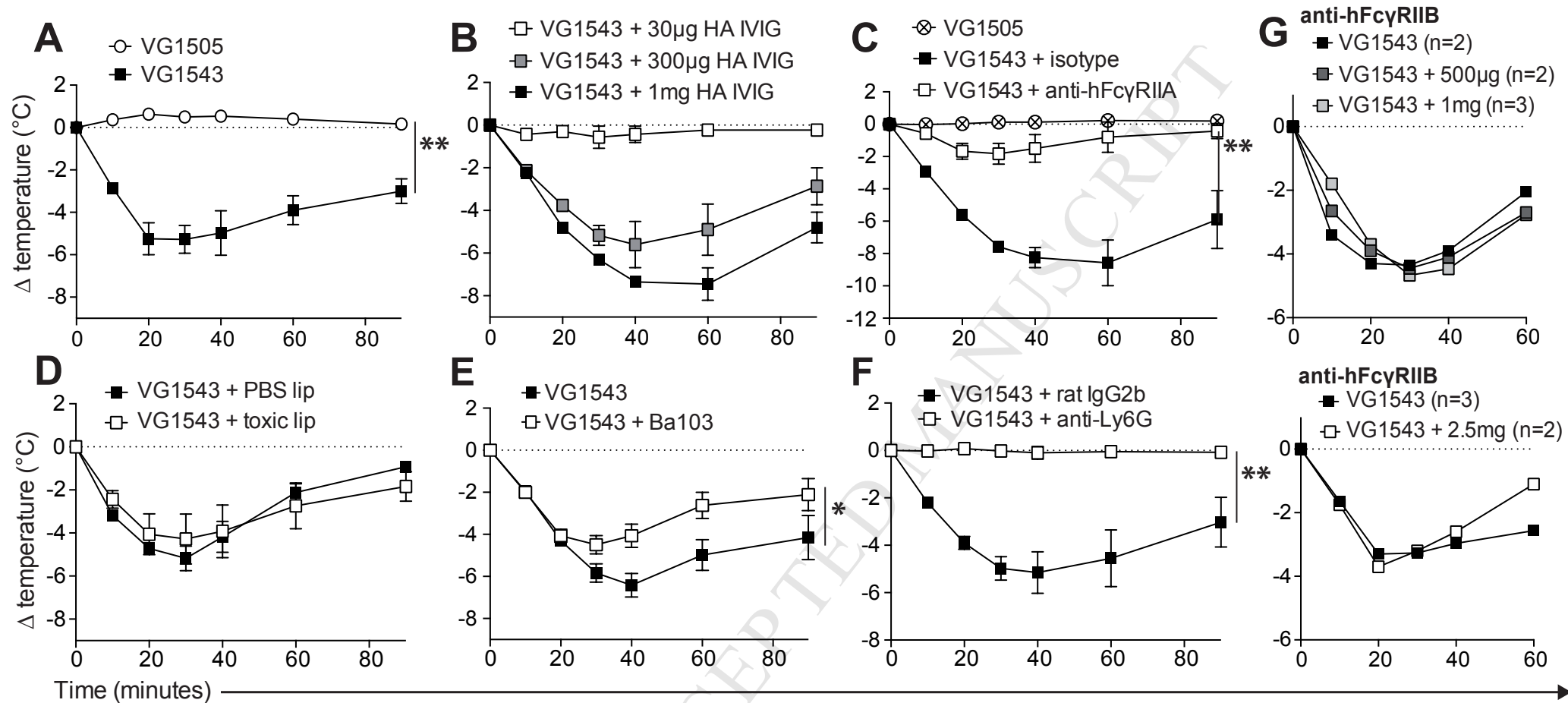
**Figure 3**

Figure 4



**Figure 5**

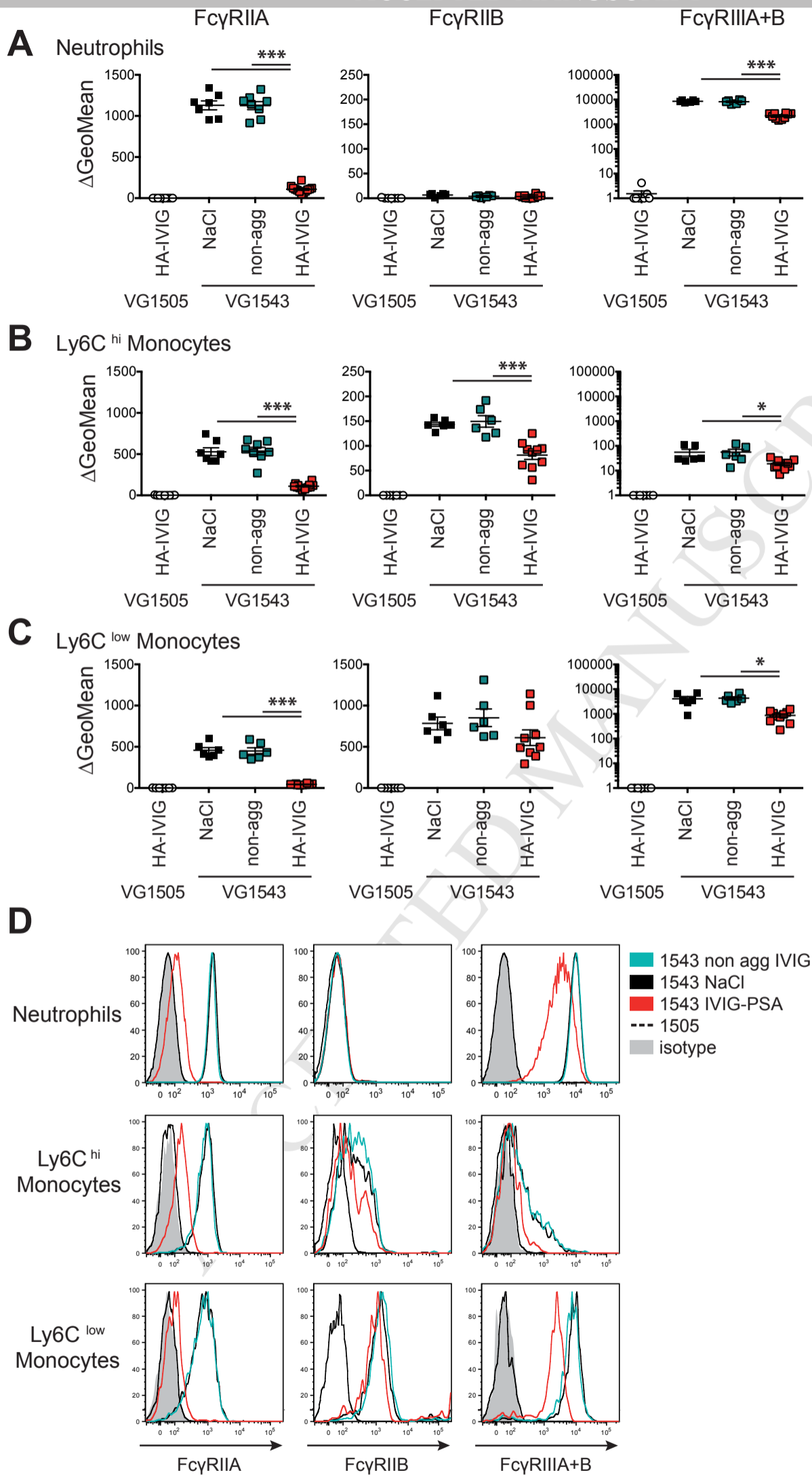
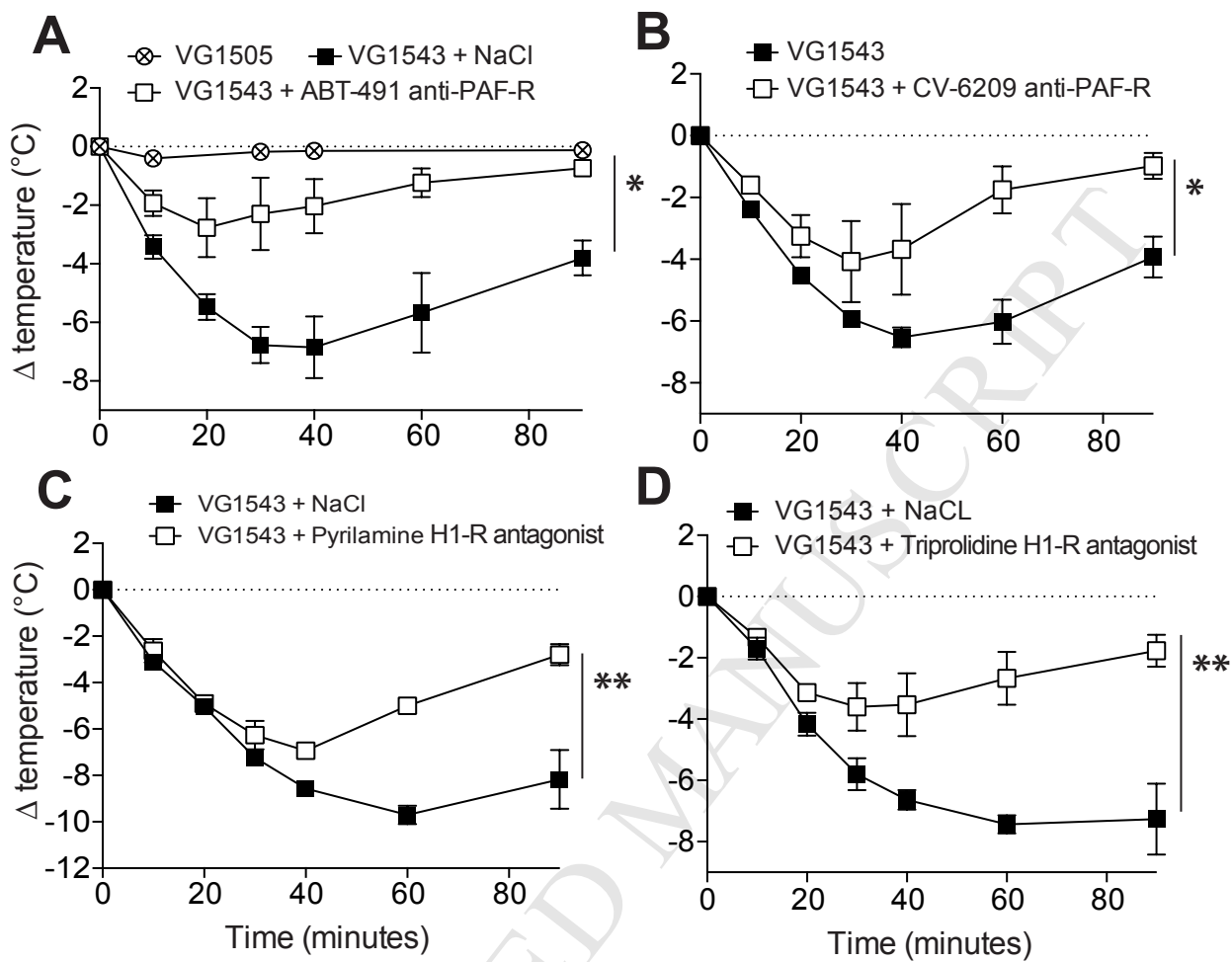


Figure 6



**SUPPLEMENTAL METHODS****Generation of mFc $\gamma$ RIIB, mFc $\gamma$ RIII and mFc $\gamma$ RIV knock-out mice.**

A targeting construct (Figure 1A) for deleting the mouse Fcgr2b, Fcgr3 and Fcgr4 genes (encoding mFc $\gamma$ RIIB, mFc $\gamma$ RIII, and mFc $\gamma$ RIV respectively) in a single targeting step was constructed by using *VELOCIGENE* technology<sup>1</sup>. Mouse sequences were obtained from bacterial artificial chromosome (BAC) clone RP23-395F6. A donor fragment was constructed by cloning a lox'd neomycin cassette flanked by site-specific recombination sites. More specifically, 5' mouse homology arm, corresponding to 270bp of mouse sequence located 3796 bp downstream of Fcgr2b, was PCR'ed using oligos (Supplemental Tables 1 and 2) and cloned upstream of a mutant lox'd neomycin selection cassette followed by a mouse 3' homology arm corresponding to 342 bp of mouse sequence (PCR using oligos noted in Supplemental Tables 1 and 2) located 4001 bp upstream of the ATG of Fcgr3. This donor fragment was inserted into Escherichia coli strain DH10B containing the mouse BAC clone RP23-395F6 and a recombination enzyme vector. Cells were grown in drug selection medium. Upon homologous recombination (BHR) at the locus, a drug selection cassette replaces the Fcgr2b, Fcgr3 and Fcgr4 genes. Individual clones were grown, and the targeted BAC DNA that contains a lox'd drug cassette in place of the Fcgr2b, Fcgr3 and Fcgr4 genes was extracted. Targeted cells were identified by PCR using up detect primer set and down detect primer set (Supplemental Tables 1 and 2). Part of the vector was sequenced to confirm proper mouse-cassette junctions and pulsed field gel electrophoresis was used to establish insert size and expected restriction fragment length.

The targeting vector (LTVEC) VG1505 was linearized and used to electroporate VGF1 mouse embryonic stem (ES) cells. Upon homologous recombination at the locus 106kb of the endogenous Fcgr2b, Fcgr3 and Fcgr4 locus is thereby deleted & replaced by lox'd

neomycin cassette resulting in an ES cell that does not express endogenous *Fcgr2b*, *Fcgr3* and *Fcgr4* genes. Correctly targeted ES cells were introduced into an eight cell stage mouse embryo by the *VELOCIMOUSE* method<sup>2</sup>. *VELOCIMICE* (F0 mice fully derived from the donor ES cell) bearing the deleted *Fcgr2b*, *Fcgr3* and *Fcgr4* genes were identified by genotyping for loss of mouse allele using a modification of allele assay (Supplemental Table 3).

### **Generation of knock-in hFcγRIIA(H<sub>131</sub>)-hFcγRIIB(I<sub>232</sub>)-hFcγRIIC(Stop<sub>13</sub>)-hFcγRIIIA(V<sub>158</sub>)-hFcγRIIIB(NA2) mice**

Targeting constructs (Figure 1B-C) for subsequent humanization of mouse mFcγRs by two sequential targeting steps, were constructed by using *VELOCIGENE* technology<sup>1</sup>. For the first targeting construct, VG1528, human sequences were obtained from bacterial artificial chromosome (BAC) clone CTD-2514J12. BACvec VG1528 was constructed in four steps as described in Supplemental Tables 1 and 2. In step 1, a donor fragment was constructed by cloning a *frt*'d hygromycin cassette flanked by site-specific recombination sites. More specifically, 5' BAC backbone homology arm, corresponding to 384bp of pBeloBAC11, was PCR'ed using oligos (Supplemental Table 1) and cloned upstream of a *frt*'d hygromycin selection cassette followed by a human 3' homology arm corresponding to 342bp of human sequence (PCR'd using oligos in Supplemental Tables 1 and 2) located 19kb upstream of the human *FCGR3A* gene (encoding hFcγRIIIA). BHR with this donor fragment deleted 41kb from the 5' end of CTD-2514J12, replacing it with an I-CeuI site and the *frt*'d hygromycin cassette to make VI209. In step 2, VI209 was modified by BHR to insert a PI-SceI site and spec cassette at the 3' end to make VI212 (Supplemental Tables 1 and 2). In step 3, RP23-395F6 was modified by BHR to delete the entire 106kb mouse low-affinity mFcγR locus (*Fcgr2b*, *Fcgr3* and *Fcgr4* genes), replacing it with a *lox*'d neomycin cassette flanked by a 5'

I-CeuI site and a 3' PI-SceI site. The extra PI-SceI site in the backbone was then deleted by AscI digestion and ligation to make VI208. In step 4, the 69kb human hFcγRs-encoding fragment from VI212 was ligated into the I-CeuI and PI-SceI sites of VI208, replacing the lox'd neomycin cassette to make the final LTVEC VG1528.

For the second targeting construct VG1543, human sequences were obtained from bacterial artificial chromosome (BAC) clone RP11-697E5. BACvec VG1543 was constructed in three steps as described in Supplemental Tables 1 and 2. In step 1, a donor fragment was constructed by cloning a spectinomycin cassette flanked by site-specific recombination sites. More specifically, 5' homology arm, corresponding to 59bp of human sequence and BAC backbone sequence that is 4558 bp downstream of FCGR3A, was ligated to a spectinomycin selection cassette followed by a 3' homology arm corresponding to 333bp of backbone sequence in pBACe3.6. BHR with this donor fragment trimmed the human hFcγR locus on the proximal end of RP11-697E5, deleting the PI-SceI site, to make VI217. In step 2, VI217 was modified by BHR using a donor fragment consisting of 5' homology arm corresponding to 258bp of BAC backbone sequence in pBACe3.6, a frt'd hygromycin cassette flanked by a 5' NotI site and a 3' PI-SceI site, and 3' homology arm corresponding to 274bp of human sequence 1188bp upstream of FCGR2B to make VI222. In step 3, the 47kb mouse distal homology arm with lox'd neomycin cassette from VI208 was ligated into the NotI and PI-SceI sites of VI222, replacing the frt'd hygromycin cassette to make the final LTVEC VG1543.

The targeting vectors were linearized and used to electroporate mouse embryonic stem (ES) cells<sup>3</sup>. Upon homologous recombination at the locus 106kb of the endogenous mouse low-affinity FcγR locus (Fcgr2b, Fcgr3 and Fcgr4 genes) is thereby deleted & replaced by human FCGR2B, FCGR3B, FCGR2C, FCGR3A and FCGR2A genes (encoding hFcγRIIB variant I<sub>232</sub>, hFcγRIIB variant NA2, hFcγRIIC variant stop<sub>13</sub>, hFcγRIIA variant V<sub>158</sub>, and



hFcγRIIA variant H<sub>131</sub>) by sequential targeting of VG1528 and VG1543, resulting in an ES cell that expresses low-affinity human hFcγR genes instead of endogenous low-affinity mouse mFcγR genes. Correctly targeted ES cells were introduced into an eight cell stage mouse embryo by the *VELOCIMOUSE* method<sup>2</sup>. *VELOCIMICE* (F0 mice fully derived from the donor ES cell) bearing the human FCGR2B, FCGR3B, FCGR2C, FCGR3A and FCGR2A genes were identified by genotyping for loss of mouse allele & gain of human allele using a modification of allele assay (Supplemental Table 3).

### **Antibodies and reagents**

Bovine serum albumin (BSA), complete and incomplete Freund's adjuvant (CFA, IFA) and ABT-491 were from Sigma-Aldrich; Cetirizine DiHCl was from Selleck Chemicals; TNP-BSA was from Santa Cruz. Fluorescently labelled anti-mouse CD11b, CD43, CD49b, CD115, CD335 (NKp46), Ly6C, Ly6G, Gr-1, B220, IgD and SiglecF were from BD Biosciences; anti-mouse CD19 and IgM from Biolegend; and anti-mouse IgE from eBioscience. Fluorescently labelled anti-human CD3, CD11b, CD14, CD15, CD19, CD56 were from Miltenyi Biotec; anti-human CD61 and CD16 (3G8) from BD Biosciences; anti-hFcγRIIA (IV.3) from Stem Cell Technologies. Fluorescently labelled anti-hFcγRIIB (2B6) in a chimeric mouse-human IgG1 N<sub>297</sub>A form was prepared in-house.

PBS-liposomes and Clodronate-liposomes were prepared as published<sup>4</sup>. The hybridoma producing mAbs anti-hFcγRIIA (IV.3) was provided by C.L. Anderson (Heart & Lung Research Institute, Columbus, OH, USA), anti-Gr1 (RB6-8C4) by R. Coffman (DNAX Research Institute, Palo Alto, California, USA), and anti-Ly-6G (NIMP-R14) by C. Leclerc (Institut Pasteur, Paris, France). mAbs were purified from hybridoma supernatants by Protein G-affinity purification. Purified mAbs anti-Ba103 were provided by H. Karasuyama (Tokyo Medical and Dental University Graduate School, Tokyo, Japan).

## Tissue processing

Cells were isolated from the blood and organs of VG1505 and VG1543 mice as follows. Spleens were dissociated through a 70µm cell strainer into MACS buffer (PBS /0.5%BSA /2mM EDTA) and RBC lysis was performed using an ammonium chloride-based buffer. For isolation of skin cells, ears were split into dorsal and ventral halves and roughly chopped before digestion with 0.25mg/mL Liberase TL ResearchGrade (Roche) + 0.1mg/mL DNase (Sigma) for 1h at 37°C (800rpm; Eppendorf Thermomixer), washed with 10x volume of PBS/10%FBS /2mM EDTA and processed through a 100µm cell strainer. Livers were perfused with cold PBS before dissection, and processed using the GentleMACS liver dissociation kit and the Octo Dissociator (Miltenyi Biotec). Cells were isolated from the peritoneum by lavage with 6mL cold PBS; BALs were performed 3x with 1mL PBS. For blood leukocyte analysis, a precise volume of heparinised blood was subjected to RBC lysis and washed with MACS buffer.

## Flow cytometry

Human EDTA-collected blood was obtained from the blood bank « Établissement Français du Sang ». After red blood cell lysis, leukocytes were stained with fluorescently labelled mAbs for 30min at 4°C. Human cell populations were distinguished as: CD15<sup>+</sup>CD193<sup>neg</sup> neutrophils; CD193<sup>+</sup>CD15<sup>low</sup> eosinophils; CD3<sup>+</sup> T cells; CD19<sup>+</sup> B cells; CD56<sup>+</sup> NK cells; CD123<sup>+</sup>CD203c<sup>low</sup>FcεRI<sup>hi</sup> basophils; CD14<sup>+</sup> monocytes; CD14<sup>hi</sup>CD16<sup>low</sup> classical monocytes and CD14<sup>low</sup>CD16<sup>hi</sup> patrolling monocytes; CD61<sup>+</sup> platelets.

Isolated single cell suspensions from mouse blood and organs were stained with fluorescently labelled mAbs for 30-40min at 4°C. Mouse cell populations were distinguished by FSC/SSC characteristics and by surface markers as follows: neutrophils (CD11b<sup>+</sup> Ly6C<sup>low</sup> Ly6G<sup>+</sup>),

monocytes (classical CD11b<sup>+</sup> Ly6G<sup>neg</sup> Ly6C<sup>hi</sup> or patrolling CD11b<sup>+</sup> Ly6G<sup>neg</sup> CD115<sup>+</sup> Ly6C<sup>low</sup>), peritoneal macrophages (CD11b<sup>hi</sup> Gr1<sup>low</sup>), alveolar macrophages (CD11c<sup>hi</sup>), liver and bone marrow macrophages (CD11b<sup>hi</sup> Gr1<sup>low</sup>F4/80<sup>+</sup>), eosinophils (CD11b<sup>+</sup> SiglecF<sup>+</sup> SSC<sup>hi</sup>), basophils (CD45<sup>low</sup> mIgE<sup>+</sup> CD49b<sup>+</sup>), mast cells (mIgE<sup>+</sup>CD49b<sup>+</sup>CD117<sup>+</sup>), platelets (CD41<sup>+</sup>), T cells (CD3<sup>+</sup>; CD4<sup>+</sup>/CD8<sup>+</sup>), B cells (CD19<sup>+</sup>/B220<sup>+</sup>, subpopulations as in Supplemental Figure 1), and NK cells (NKp46<sup>+</sup>CD49b<sup>+</sup>).

hFc  $\gamma$  RIIA was identified by the specific mAb clone IV.3. hFc  $\gamma$  RIIIB was identified by the clone 2B6<sup>5</sup>, expressed as a chimeric mouse-human IgG1 N<sub>297</sub>A variant to inhibit unspecific binding via the Fc portion of the antibody. We used an anti-CD16 antibody (clone 3G8) to characterise jointly hFc  $\gamma$  RIIIA and hFc  $\gamma$  RIIIB expression, because we could not identify, using a series of commercially available anti-CD16 antibodies, an antibody able to distinguish surface expression of hFc  $\gamma$  RIIIA(V<sub>158</sub>) from hFc  $\gamma$  RIIIB(NA2). In supplemental figure 7: anti-CD32 clone FLI8.26 defines hFc $\gamma$ RIIA+B expression; anti-CD32(R131) clone 3D3 defines hFc $\gamma$ RIIB expression only, because VG1543 mice express the H131 variant of hFc $\gamma$ RIIA; anti-CD16 clone MEM-154 defines hFc $\gamma$ RIIA+B expression. mFc $\gamma$ RI was identified using the specific clone X54-5/7.1 (BD Biosciences).

For *ex vivo* binding of cells with human IgG, blood cell suspensions were incubated first with aggregated IVIG (20  $\mu$ g/mL) for 1 hour on ice, and then stained with a fluorescently labelled antibody cocktail, including anti-human IgG Fab-specific goat F(ab')<sub>2</sub> fragment (Jackson ImmunoResearch). Cells isolated from VG1543 mice after IVIG-PSA were stained with the secondary antibody alone.

Samples were run on a MACSQuant flow cytometer (Miltenyi) and data analysed using FlowJo Software (Treestar Inc.).

**Specificity and efficiency of cell depletion strategies:**

Appropriate antibody-mediated cell depletion using anti-Ly6G (NIMP-R14) and anti-CD200R3 (Ba103) was examined by flow cytometry analysis. NIMP-R14 treatment (300 $\mu$ g) efficiently depleted neutrophils in the blood, spleen and peritoneum. The percentage of total CD11b<sup>+</sup>CD115<sup>+</sup> monocytes in the blood and CD11b<sup>+</sup>Gr1<sup>int</sup> monocytes in the spleen were unaffected, while the percentage of CD11b<sup>+</sup>F4/80<sup>+</sup> macrophages in the peritoneum increased slightly. The percentage of blood basophils was slightly increased, but total numbers were unaffected and spleen basophils and peritoneal mast cells were not affected. We did, however observe that the frequency of Ly6C<sup>hi</sup> monocytes decreased while the frequency of Ly6C<sup>low</sup> monocytes increased following NIMP-R14 treatment, a phenomenon which may reflect epitope masking by NIMP-R14 due to a low-level cross-recognition. NIMP-R14 therefore efficiently depletes neutrophils with some effects on other cell populations. Ba103 administration at 30 $\mu$ g per mouse induced basophil depletion in the blood and spleen, without affecting circulating neutrophils and monocytes (data not shown), or peritoneal mast cells. Yet the depletion of basophils was incomplete (up to 70%), and not uniformly efficient across individuals (Supplementary Figure 5A). We therefore administered Ba103 at a two-fold greater dose (60 $\mu$ g/mouse). Although we could not detect a significant increase in depletion compared to the 30 $\mu$ g dose (data not shown), this increased dose indicated a minor contribution of basophils to anaphylaxis severity (Figure 4E).

We have previously demonstrated efficient monocyte/macrophage depletion in the blood and spleen following intravenous liposome injection (Beutier et al 2016. JACI *in press*); whereas peritoneal macrophages remained intact. In efforts to achieve complete monocyte/macrophage depletion, we combined multiple injections of clodronate liposomes with different routes of administration, resulting in higher total liposome load: these approaches were inconclusive, however, and while we were efficiently able to deplete resident macrophages, we observed

increases in numbers of circulating inflammatory monocytes, and wildly inconsistent responses during IVIG-PSA. Indeed, toxic liposomes can affect all phagocytic cell populations, and approaches to increase their efficacy also augment non-specific effects. For this study, we confirmed that the ability of macrophages to mediate thrombocytopenia (reflecting capacity to engage and engulf antibody-bound cells, and by logical extension, immune complexes) remains intact following antibody-mediated depletion strategies (*e.g.* NIMP-R14 or Ba103), but is blocked following intravenous clodronate liposome injection at the doses used herein.

### Statistics

Statistical analyses were performed using Prism. Survival was analysed by a log-rank (Mantel-Cox) test to compare test subjects and controls. Temperature loss during ASA was compared using a Student's t-test of individual time points. Temperature loss during PSA was compared by 2-way repeated measures ANOVA (RM-ANOVA), except in Supplementary Figure 8E in which groups were compared using a Student's t-test at 30min. hFcγR expression in Figure 5 and Supplementary Figure 7 was compared using an unpaired t-test with Welch's correction for unequal variances.

### Supplemental References

1. Valenzuela DM, Murphy AJ, Friendewey D, Gale NW, Economides AN, Auerbach W, et al. High-throughput engineering of the mouse genome coupled with high-resolution expression analysis. *Nat Biotechnol* 2003; 21:652-9.
2. Poueymirou WT, Auerbach W, Friendewey D, Hickey JF, Escaravage JM, Esau L, et al. F0 generation mice fully derived from gene-targeted embryonic stem cells allowing immediate phenotypic analyses. *Nat Biotechnol* 2007; 25:91-9.
3. Auerbach W, Dunmore JH, Fairchild-Huntress V, Fang Q, Auerbach AB, Huszar D, et al. Establishment and chimera analysis of 129/SvEv- and C57BL/6-derived mouse embryonic stem cell lines. *Biotechniques* 2000; 29:1024-8, 30, 32.
4. Van Rooijen N, Sanders A. Liposome mediated depletion of macrophages: mechanism of action, preparation of liposomes and applications. *J Immunol Methods* 1994; 174:83-93.
5. Veri MC, Gorlatov S, Li H, Burke S, Johnson S, Stavenhagen J, et al. Monoclonal antibodies capable of discriminating the human inhibitory Fcγ-receptor IIB (CD32B) from the activating Fcγ-receptor IIA (CD32A): biochemical, biological and functional characterization. *Immunology* 2007; 121:392-404.

## SUPPLEMENTAL FIGURE LEGENDS

**Supplemental Figure 1: VG1505 and VG1543 mice demonstrate normal immune cell composition of major compartments, and comparable expression of mFcεRI and mFcγRI.**

(A) Spleens taken from VG1505 mice and VG1543 mice were comparable in size. (B) Leukocyte counts in total blood were enumerated using an automatic blood cell analyser and (C; see also supplementary table 4) frequency of blood immune cell populations was determined by flow cytometry. (D) mFcεRI expression on peritoneal mast cells from VG1505 mice and VG1543 mice: representative histograms are shown and values represent  $\Delta$ GeoMean between specific staining and isotype control. (E) Anti-IgE staining on basophils in the blood, spleen and bone marrow, as a surrogate measure of mFcεRI expression. (F) Representative histograms showing mFcγRI expression on various monocyte and macrophage populations isolated from VG1505 mice and VG1543 mice.

**Supplemental Figure 2: Variability in hFcγR expression on monocytes and eosinophils from different human blood donors. B cells and monocytes exhibit subpopulation-distinct variation in hFcγR expression.**

Cells were isolated from the (A, E, F) blood of healthy human donors, or (B) bone marrow, (C) peritoneum, or (D) blood of VG1543 mice, for flow cytometry analysis. (A) Variable expression hFcγRIIB on monocytes from the blood of 4 different human donors; numbers indicate frequency of cells positive for FcγR staining. (B, C) Representative histograms showing hFcγRIIB expression on VG1543 B cell subpopulations: (B) mature B cells (B220<sup>hi</sup> CD43<sup>neg</sup> IgM<sup>+</sup> IgD<sup>+</sup>) and (B220<sup>low</sup> CD43<sup>neg</sup>) immature (IgM<sup>+</sup>), pro (IgM<sup>neg</sup>) and pre (IgM<sup>neg</sup> IgD<sup>neg</sup>) B cells from the bone marrow, and (C) peritoneal B1a cells (IgM<sup>+</sup> CD11b<sup>+</sup> IgD<sup>low</sup>) and B2 cells (IgM<sup>+</sup> CD11b<sup>neg</sup> IgD<sup>hi</sup>). Numbers indicate  $\Delta$ GeoMean between specific staining and FMO controls. Data is representative of at least 2 independent experiments, n>3. (D, E) Discrimination of classical vs patrolling monocyte subsets in the blood of VG1543 mice (D) or human donors (E); differential hFcγRIIA, hFcγRIIB and hFcγRIII expression on monocyte subsets is shown by representative histograms. Shaded grey histograms indicate background staining from VG1505 mice; shaded blue histograms indicate background staining with an isotype control antibody (hFcγRIIA, hFcγRIII), or an FMO control (hFcγRIIB). (F) Variable expression of hFcγRIII on eosinophils from the blood of 4 different human donors

**Supplemental Figure 3: Immunisation with BSA in CFA/IFA induces BSA-specific IgG1 and IgG2 in VG1505 and VG1543 mice.**

(A) Anti-IgG1 and (B) anti-IgG2a/b/c BSA-specific ELISA results from two independent experiments are represented as serial dilution curves of individual mouse sera, and as average curve (insets). VG1505 (dashed black line) and VG1543 (solid black line) mice exhibit comparable antibody titres; excl\*\* (blue line) indicates mice that were excluded from challenge due to low antibody titres; positive (pos: red line) and negative (neg: dotted black line) ELISA controls are indicated.

**Supplemental Figure 4: Antibody clone NIMP-R14 specifically targets Ly-6G antigen and efficiently depletes neutrophils *in vivo*.**

(A-C) Blood sampled from naive mice (pool of n=4) was stained with FITC-conjugated NIMP-R14 in combination with fluorescent antibody clones 1A8 (anti-Ly-6G; A), RB6-8C5 (anti-GR1: binds Ly-6C and Ly-6G; B), or anti-Ly-6C (Monts 1; C) with or without pre-blocking with an excess of unconjugated NIMP-R14 or 1A8. Staining was assessed by flow cytometry, and representative plots are shown pre-gated on single, live CD11b<sup>+</sup> cells. (D-F) VG1543 mice were treated with 300µg NIMP-R14 or rat isotype control antibody (rIgG2b) and blood and tissues were sampled 24 hours later and frequencies of specific cell populations determined by flow cytometry: gating strategies are shown and frequencies of neutrophils and monocyte/macrophages in the (D) blood, (E) spleen and (F) peritoneum; and percentage of basophils in the (G) blood and (H) spleen, and (I) mast cells in the peritoneum. (D-F) Data is pooled from 2 independent experiments.

**Supplemental Figure 5: Basophils, monocyte/macrophages and histamine were not found to contribute to BSA-ASA in VG1543 mice.**

(A) VG1543 mice were treated with 30µg anti-CD200R3 (Ba103) or rat isotype control antibody (rIgG2b) and blood and tissues sampled 24 hours later: representative gating strategy and percentage of basophils in the blood and spleen; and percentage of mast cells in the peritoneum. (B-G) Change in body temperature and survival during BSA-ASA in VG1505 and VG1543 mice, and VG1543 mice treated with (B) anti-GR1 mAbs, (C&E) toxic liposomes, (D) anti-CD200R3 mAbs, (F) H1-receptor antagonist Cetirizine, (G) PAF-R antagonist ABT-491, or respective controls. Data are represented as mean ± SEM and are representative of at least 2 independent experiments. (E) BSA-ASA with high mortality in VG1543 mice treated with PBS or toxin-containing liposomes before challenge: repeat of panel 5C. (G) BSA-ASA with no mortality in VG1543 mice treated or not with PAF-R antagonist before challenge: repeat of Figure 3D.

**Supplemental Figure 6: PSA-induced hypothermia of VG1543 mice after injection of high-dose heat-aggregated IVIG, or basophil depletion**

(A) VG1543 mice were injected with indicated amounts of heat-aggregated IVIG and central temperatures monitored. Data are represented as individual replicates of each dose. (B) VG1543 mice treated with 30µg anti-CD200R3 (Ba103) or isotype control 24 hours before injection of 1mg heat aggregated IVIG and PSA induction.

**Supplemental Figure 7: Observed reduction in hFcγR expression on circulating myeloid cell populations after IVIG-PSA is not due to binding inhibition by surface bound hIgG.**

hFcγR expression on blood (A) neutrophils, (B) Ly6C<sup>hi</sup> and (C) Ly6C<sup>low</sup> monocytes from VG1543 mice 1 hour after injection of non-aggregated IVIG (non-agg) or heat aggregated-IVIG (HA-IVIG, leading to PSA). Only non-blocking antibodies were used for detecting hFcγR expression, to avoid competition with ligand (*i.e.* IVIG) binding: anti-CD32 clone FLI8.26 defines hFcγRIIA+B expression, anti-CD32(R131) clone 3D3 defines hFcγRIIB expression, and anti-CD16 clone MEM-154 defines hFcγRIIIA+B expression. Background

staining on cells from VG1505 mice is shown 1 hour after injection of heat aggregated-IVIG. Values represent GeoMean of specific staining, pooled from three independent experiments. (\*\*p<0.001, \*\*p<0.01, Student's t test). (D) Staining of surface hIgG bound *ex vivo* by incubating blood neutrophils and monocytes isolated from (left histograms) naïve VG1543 mice or (central histograms) PAF-injected VG1543 mice (0.3µg PAF injected i.v. to induce PAF-dependent anaphylaxis) with HA-IVIG (20µg/mL). These histograms were compared to histograms (right) representing staining of surface hIgG bound *in vivo* to blood cell populations, isolated 1 hour after IVIG-PSA. Representative histograms are shown from 2-3 independent experiments, n≥3. Shaded histograms represent labelling with secondary antibody alone (left and central panels) or FMO control (right panels).

**Supplemental Figure 8: Role of mediators in PSA.** (A-C) Antihistamine treatment inhibits IgE-PSA: VG1505 mice were sensitised by transfer of anti-TNP specific IgE and challenged with TNP-BSA. Indicated mice were injected i.p. with H1 receptor antagonists (A) cetirizine 300µg or (B) pyrilamine 300µg 30min prior, or (C) triprolidine 200µg 20min prior to challenge. *NB* triprolidine was injected at 200µg/mouse in (C): this dose was increased to 300µg for IVIG-PSA pretreatment (Figure 6D). (D-E) VG1543 were treated (D) with cetirizine alone or (E) in combination with PAF-R antagonist ABT-491 prior to IVIG-PSA. Data is (D) representative or (E) collated from 6 independent experiments. \*\*\*p<0.001, VG1543 controls vs VG1543 + PAF-R antagonist and VG1543 controls vs VG1543 + PAF-R antagonist + antihistamine, \*\* p<0.05 VG1543 + PAF-R antagonist vs VG1543 + PAF-R antagonist + antihistamine, Student's t-test at 30min. (F) Administration of PAF-R antagonist ABT-491 at an increased dose does not confer increased protection from IVIG-PSA: VG1543 were injected i.v. with 25 or 100µg of PAF-R antagonist ABT-491 15 min before the induction of IVIG-PSA.



Supplementary Table 1: Bacvec description

BAC vec	Step	Description	Cassette	Recipient BAC	Process	Product name	Drug selection	primers for detection
1505	1	Deletion of the mouse low FCGRs, deleting 106kb (fig 1).	[mFcR 5' up (1)/mFcR 3' up XbaI (1a)]-ICeu1-PGKp-em7-neoR-pA-lox2372-[5' down Sac1/mFcR 3' down]	RP23-395f6	BHR	1505	kan cm	mFcR 5'up detect(3), mFcR 3'down detect
1528	1	Trim human FCGR locus on the distal end of human BAC CTD2514j12, insert a ICeu1 site at the distal end, deleting 41kb.	[5' down loxp pbelo/3' del loxp (KpnI)]-ICeu1-frt-UbCp-em7-hyg-pA-[5' down primer-SacI (h14)/3' down primer (h15)]	CTD2514j12	BHR	VI-209	hyg cm	5'pbelo loxp detect, 3' down detect (h16)
	2	Insert PI-Sce1 site into the proximal end human BAC construct VI-209.	[5' up primer (h4)/3' up primer XhoI (h5)]-PI-Sce1-Spec-[del cm (AvrII)/3' up homology CM pbelo]	VI-209	BHR	VI-212	hyg spec	5'up detect (h6), 3' pbelo-cm detect
	3	Deletion of the mouse low FCGRs (106kb) and inserted ICeu1 and PI-Sce1 sites flanking neoR (VI207), and then removed the extra PI-Sce1 site by Asc1, digestion and ligation to make VI208.	[mFcR 5' up (1)/3' up mFcR-2b NheI primer (2) [Rev]]-ICeu1-loxp-PGKp-em7-neoR-pA-loxp-PI-Sce1[mFcR 5' down ApaI(7) [Rev]/mFcR 3' down]	RP23-395f6 and VI207	BHR, Digestion /ligation	VI207 and VI208	kan cm	mFcR 5'up detect(3), mFcR 3'down detect
	4	Ligate human FCGR fragment 72.3kb from VI212 into VI208 replacing neoR.	VI212: ICeu1-hygR-72.3 kb of human FCGRs-PI-Sce1	VI208	ligation	1528	cm hyg	mFcR 5'up detect (3), mFcR 3' down detect(9)
1543	1	Trim human FCGR locus on the proximal end of human BAC RP11-697e5, deleting PI-Sce1 site (fig 3).	[5'up-(h40)/3'up-AvrII(h42)]-specR-[5' kpn del loxp bac3.6 (B10a)1[Rev]/5' down loxp pbelo1[Rev]]	RP11-697e5	BHR	VI-217	spec cm	5'up detect (h41), 5'del loxp detect (b14)1[Rev]
	2	Insert Not1 and PI-Sce1 sites flanking hygR at the distal end of VI217.	[3' up homology CM pbelo1[Rev]/5' pbelo del cm Nsi1 w/Not11[Rev]]-Not1-Pgk-hygR-PI Sce1[5' down SalI (h10)1[Rev]/3' down (h11)1[Rev]]	VI-217	BHR	VI-222	hyg spec	3'pbelo del cm detect1[Rev], 3'down detect (h12)1[Rev]
	3	Ligate mouse distal homology arm 47kb from VI-208 into VI222 replacing hygR.	Not1-PGKp-em7-neoR-pA-lox2372-47 kb of human FCGRs-PI Sce1	VI-222	ligation	1543	neo spec	3' pbelo del cm detect, 3'down detect (h12)

**Supplementary Table 2: List of primers**

Primer name	Sequence (5'-3')
mFcR 5' up (1)	ACCAGGATATGACCTGTAGAG
mFcR 3' up XbaI (1a)	TGTTTCTACTTACCCATGGAC
mFcR 5' up detect(3)	ATCCTGAGTATACTATGACAAGA
5' down Sac PI Sce	CATGCATCTATGTCGGGTGCGGAGAAAGAGGTAATGCATTCTTGCCCAATACTTAC
mFcR 3' down	CCCTCTAGCTAGGTTATTAGG
mFcR 3' down detect	GGAGCCTCAACAGGACTCCAT
5' down loxp pbelo	ATCCGATGCAAGTGTGTCGCT
3' del loxp (KpnI)	CTCGCTTTCAGCACCTGTCGT
5'pbelo loxp detect	CTGTAGAACGGAGTAACCTCG
3' down detect (h16)	CCCAGGTAAGTCGTGATGAAACAG
5' down primer-SacI (h14)	GCCAGCCACAAAGGAGATAATC
3' down primer (h15)	GCAACATTTAGGACAACCTCGGG
5' up detect (h6)	CACACATCTCCTGGTGACTTG
3' pbelo-cm detect	ACAGCATGTGCATCGCATAGG
5' up primer (h4)	GATTTCTAACCACCTACCCC
3' up primer XhoI (h5)	CAACTGCCATTGGAAAAGA
5'up-(h40)	GAATGAATTCCGCGGATCCTTCTATAGTGTCACCTAAATGTCGACGGCCAGGCAGCCGC
5'up detect (h41)	GAGCAGCCATCTATAGACCTAC
5' kpn del loxp bac3.6 (B10a)2[Rev]	CTTATCGATGATAAGCTGTCA
5' down loxp pbelo2[Rev]	ATCCGATGCAAGTGTGTCGCT
5' del loxp detect (b14)2[Rev]	TCGTGTTGTCGGTCTGATTAT
3' up homology CM pbelo2[Rev]	CAATCCAGGTCCTGACCGTTC
5' pbelo del cm nsi w/notii2[Rev]	GCCCGGTAGTGATCTTATTTT
3' pbelo del cm detect2[Rev]	ACAGCATGTGCATCGCATAGG
5' down SalI (h10)2[Rev]	AAATACACACTGCCACAGACAG
3' down (h11)2[Rev]	CACAGGAAACTCACAAAAGAGG
3'down detect (h12)2[Rev]	CTTTTTATGGTCCCACAATCAG
mFcR 3' down detect(9)	ACTCATGGAGCCTCAACAGGA
mFcR 5' down ApaI(7) [Rev]	GCATTCTTGCCCAATACTTAC
3' up mFcgR-2b NheI primer (2) [Rev]	GTTTCTACTTACCCATGGAC

**Supplementary Table 3: list of taqman probes**

Taqman probe	Description	Forward primer (5'-3')	TaqMan probe (5'-3')	Reverse Promer (5'-3')	Probe copy numbers	
					Mod	WT
Fcgr4	Fcgr2b	CCAGGGTCTCCATCCATGTT	CCACCGTGGCATCA	TCCTATCAGCAGGCAGAATGTG	0	1
Fcgr2b-U	Fcgr2b	AGCAGTGCTGCCTCCTTCC	TGACCATCGTGGAAGCCAGCCT	GGTTTGTTCCTTTGCCAGTATG	0	1
Neo	Neo gene	GGTGGAGAGGCTATTCGGC	TGGGCACAACAGACAATCGGCTG	GAACACGGCGGCATCAG	0	1
1528 hT1	Fcgr2b	TCATCACGACTTACCTGGGTTT	CCCTCCTGGTGTCCCTCTGATGAC	GGACAGGTGAAGACAGAGGAG	1	0
1528 hT1	Fcgr2b	TCCTTCCTGGTCTGTTCTATG	TCCCTTGCCAGACTTCAGACTGAGA	CTCTGTCACCCACCAATTTCC	0	0
Hyg	Hyg	TGCGGCCGATCTTAGCC	ACGAGCGGGTTTCGGCCCATTC	TTGACCGATTCTTTCGGG	0	0
1543hD	Fcgr2b	GTTCTGGTAATTGGGCTCTTTGTTC	TCTGGAGCTTCCGACTGCATAAGCAG	ACTGCTGGTTTCTGCCTTCTC	0	0
1543hU	Fcgr2b	GGGAGAATAGCAGAGCAGGAC	TCAGCAATCTCCACTCAGGGCTCA	ACACAAGTTCACGGGAAGTCAAAC	0	0
1543 AS 129	Fcgr2b	TTTCTTGCCCCAAATTGAAGA	CTCCCAAATGAATG	TCAGGCAGTCGATCTCTGTTTC	0	0
1543 AS B6	Fcgr2b	TTTCTTGCCCCAAATTGAAGA	CTCCCAAATGAGTGGAG	TCAGGCAGTCGATCTCTGTTTC	1	0
1543 AS2 129	Fcgr4	TTCTTGTTCTCCTTTGCCTCTAA	ATCCACTTAGACTGCAC	TTGAAGCTCTGCACAGTGAGATC	1	0
1543 AS2 B6	Fcgr4	TTCTTGTTCTCCTTTGCCTCTAA	TATCCACCTAGACTGC	TTGAAGCTCTGCACAGTGAGATC	1	0
1543 AS3 129	Fcgr4	GGCAGGACAGTGATAAATTCTGAGA	TGGCCCTTGCTGTGA	GGCCAAGAATGGAACATGACTT	1	0
1543 AS3 B6	Fcgr4	GGCAGGACAGTGATAAATTCTGAGA	TGGCCCTTGCTATGA	GGCCAAGAATGGAACATGACTT	1	0
					1	0

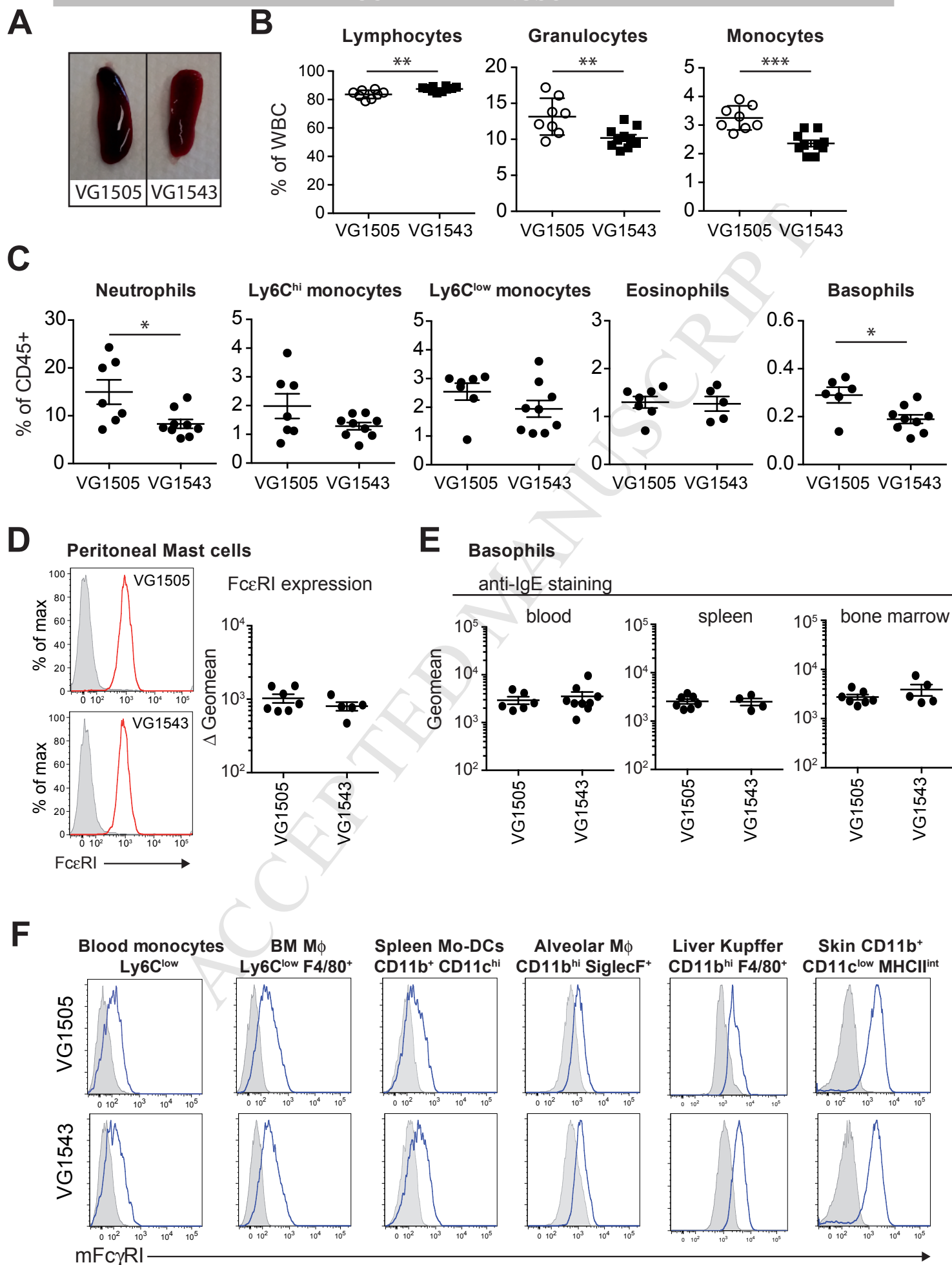
**Supplementary Table 4: Immune cell composition in VG1505 and VG1543 mice, by flow cytometry analysis**

ACCEPTED MANUSCRIPT

	VG1505	VG1543	
<b>Blood</b>			
CD19+	31,09 ± 2,012, n=7	36,48 ± 3,342, n=5	n.s.
CD4+	23,47 ± 2,489, n=7	28,24 ± 1,620, n=5	n.s.
CD8+	14,89 ± 0,9485, n=7	14,46 ± 1,006, n=5	n.s.
Neutrophils CD11b+ Ly6G+	14,97 ± 2,550, n=7	8,306 ± 0,9350, n=9	* p=0,0412
Monocytes CD11b+ (Ly6G neg) CD115+ Ly6C low-int	2,544 ± 0,2942, n=7	1,947 ± 0,2914, n=9	n.s.
Monocytes CD11b+ (Ly6G neg) CD115+ Ly6C hi	1,981 ± 0,4293, n=7	1,284 ± 0,1263, n=9	
Eosinophils CD11b+ SSC hi SiglecF+	1,299 ± 0,1207, n=7	1,266 ± 0,1527, n=5	n.s.
Basophils CD45 low IgE+ DX5+	0,2900 ± 0,03281, n=6	0,1894 ± 0,01816, n=9	* p=0,0123
<b>Bone Marrow</b>			
Neutrophils CD11b+ Ly6G int-hi	56,21 ± 3,956, n=7	45,80 ± 1,382, n=5	n.s.
Monocytes CD11b+ (Ly6G neg) Ly6C hi	8,803 ± 1,020, n=7	9,512 ± 0,6939, n=5	n.s.
Monocytes CD11b+ (Ly6G neg) Ly6C int	1,419 ± 0,2171, n=7	1,696 ± 0,1661, n=5	n.s.
Macrophages CD11b+ (Ly6G neg) Ly6C low F4/80+	1,494 ± 0,3950, n=7	1,706 ± 0,1856, n=5	n.s.
Basophils CD45 low IgE+ DX5+	0,5009 ± 0,03961, n=7	0,6222 ± 0,05160, n=5	n.s.
<b>Spleen</b>			
CD19+	37,57 ± 1,717, n=7	39,50 ± 3,019, n=5	n.s.
CD4+	15,60 ± 1,780, n=7	27,88 ± 1,423, n=5	*** p=0,0005
CD8+	9,691 ± 1,060, n=7	11,18 ± 0,6511, n=5	n.s.
Neutrophils CD11b+ Ly6G int-hi	7,900 ± 2,492, n=7	1,466 ± 0,1149, n=5	n.s.
Monocytes CD11b+ (Ly6G neg) CD115+ Ly6C low-int	1,028 ± 0,1689, n=7	0,7142 ± 0,07172, n=5	n.s.
Monocytes CD11b+ (Ly6G neg) CD115+ Ly6C hi	1,662 ± 0,5531, n=7	0,6308 ± 0,1815, n=5	n.s.
Eosinophils CD11b+ SSC hi SiglecF+	1,146 ± 0,1922, n=7	0,4212 ± 0,05560, n=5	* p=0,0116
Basophils CD45 low IgE+ DX5+	0,2484 ± 0,02648, n=7	0,1325 ± 0,005172, n=4	* p=0,0106
<b>Peritoneum</b>			
CD117+IgE+ Mast Cells	3,751 ± 0,3780, n=7	3,958 ± 1,133, n=5	n.s.
CD11b hi F480+ Macrophages	45,57 ± 3,675, n=7	20,18 ± 2,848, n=5	*** p=0,0005

# Supplementary Figure 1

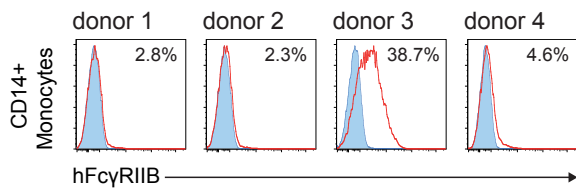
ACCEPTED MANUSCRIPT



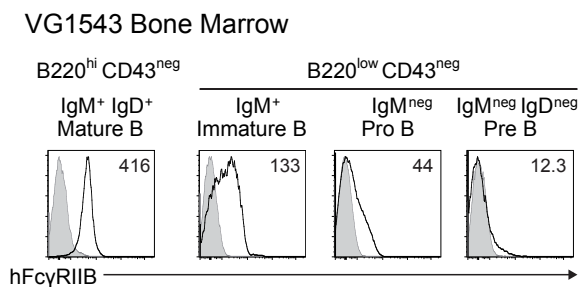
# Supplementary Figure 2

ACCEPTED MANUSCRIPT

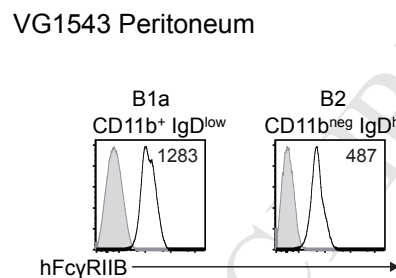
**A**



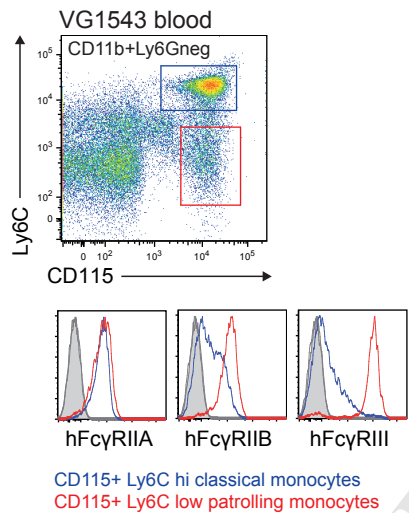
**B**



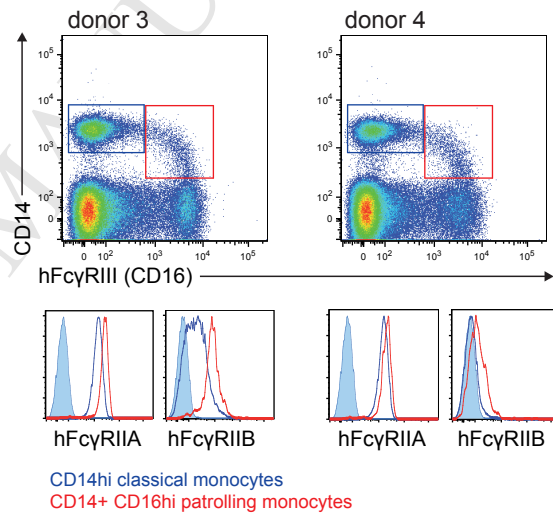
**C**



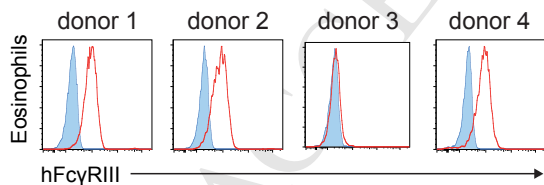
**D**



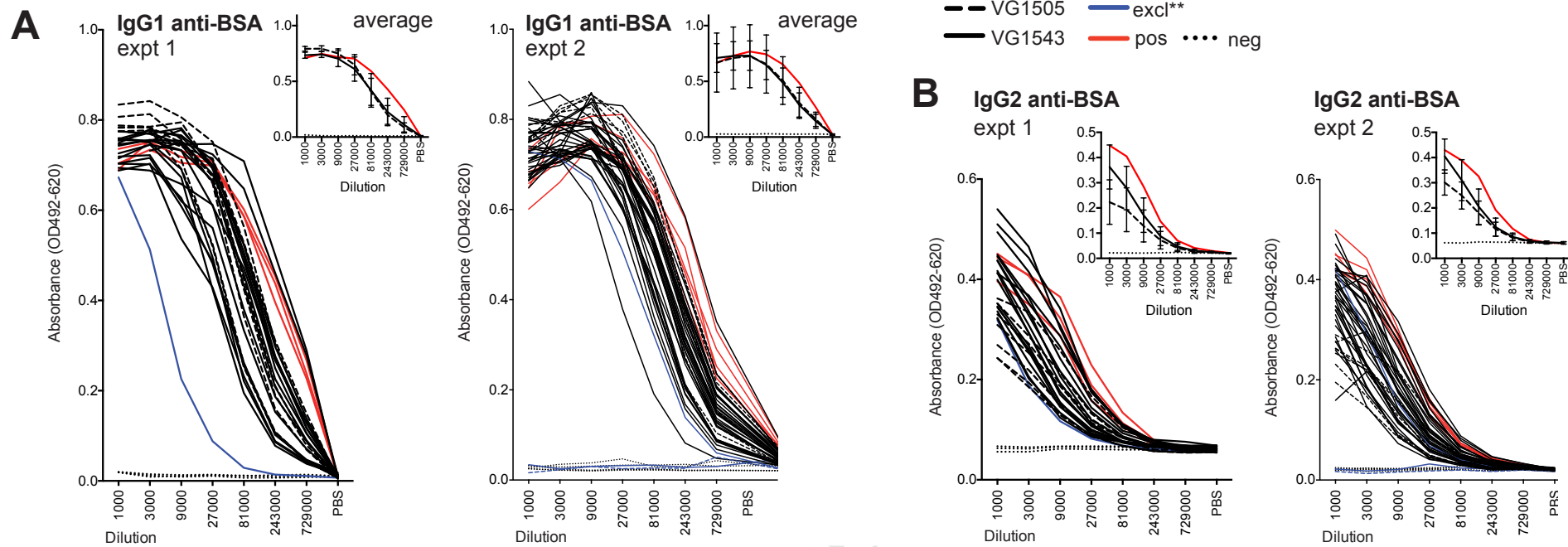
**E**



**F**

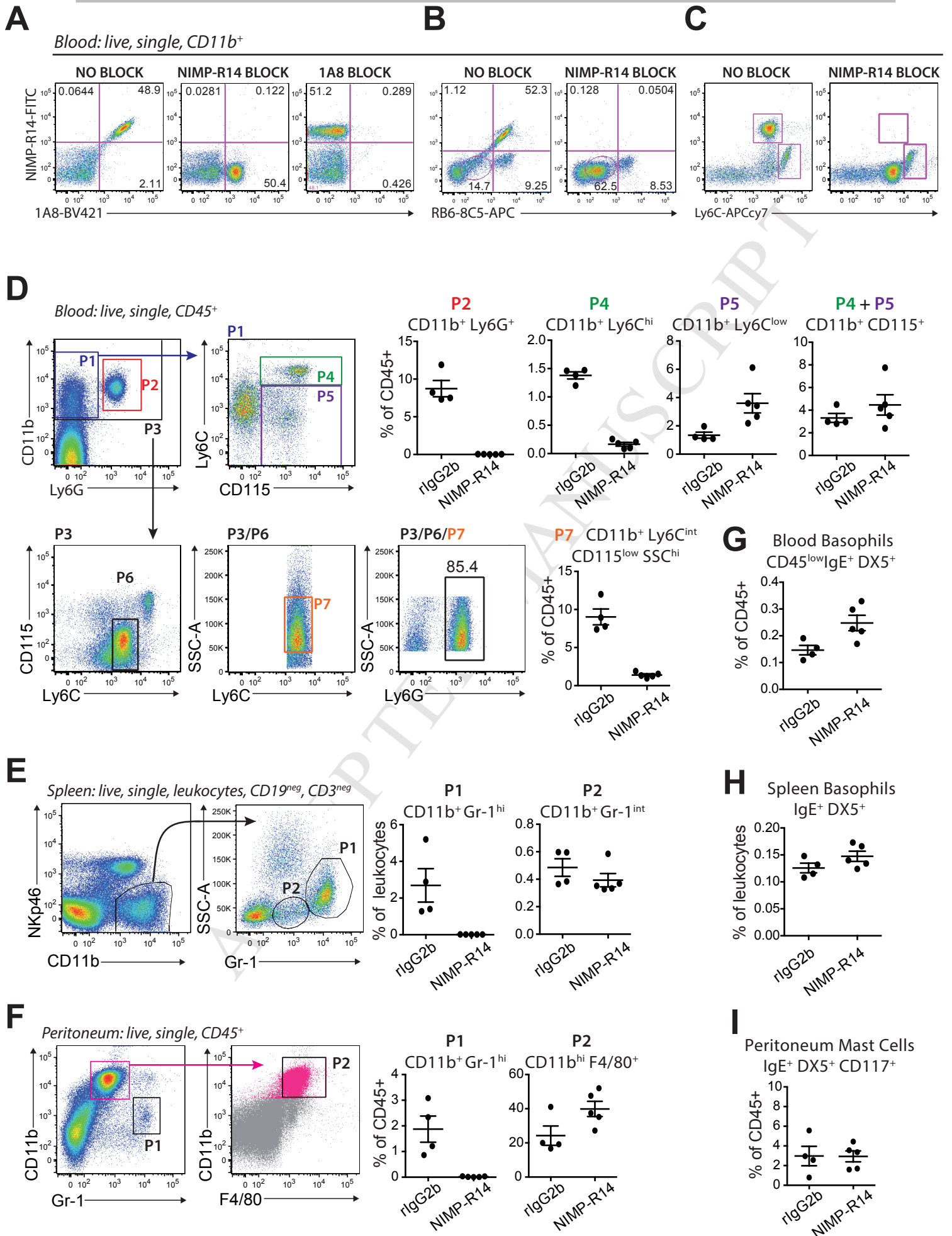


## Supplementary Figure 3



# Supplementary Figure 4

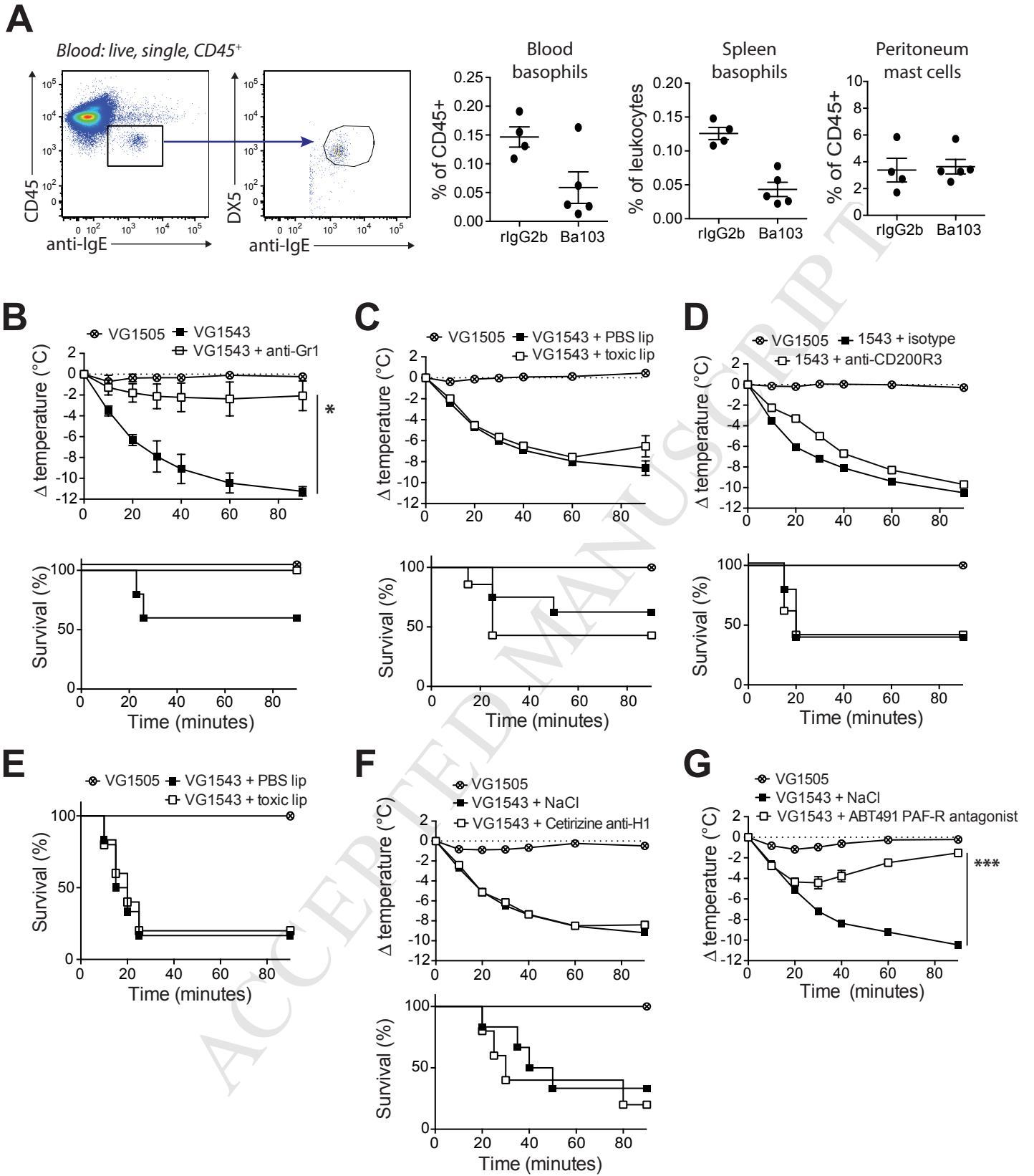
ACCEPTED MANUSCRIPT



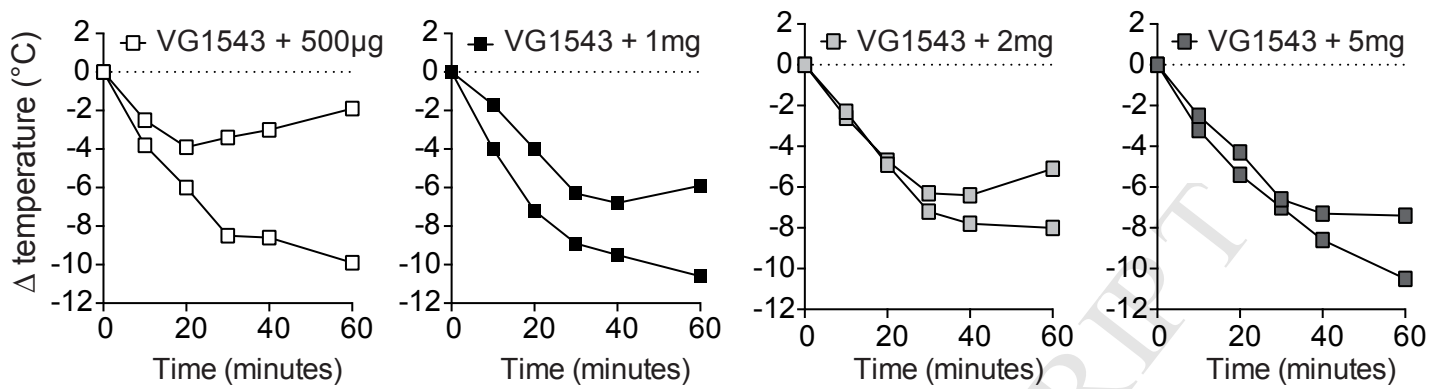


# Supplementary Figure 5

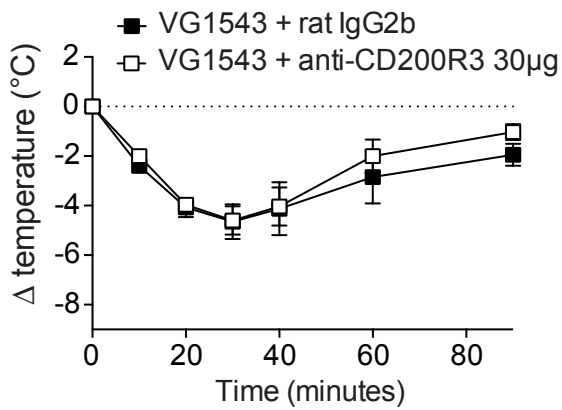
ACCEPTED MANUSCRIPT



**A**



**B**



# Supplementary Figure 7

ACCEPTED MANUSCRIPT

